Links between southwestern tropical Indian Ocean SST and precipitation over Southeastern Africa over the last 17 kyr

Syee Weldeab[1,*], David W. Lea[1], Hedi Oberhänsli[2], Ralph R. Schneider[3]

[1]Department of Earth Science, University of California, Santa Barbara, 93106, USA

[2]Museum für Naturkunde, Leibniz-Institut für Biodiversity and Evolutionsbiologie, Invalidenstrasse 43, 10115 Berlin, Germany

[3]Institute of Geoscience, Christian-Albrechts Universitaet, Kiel, Germany

*Corresponding author: weldeab@geol.ucsb.edu (S. Weldeab)

Abstract

Time series of Mg/Ca, Ba/Ca, and $\delta^{18}O$ analyzed in tests of surface-dwelling planktonic foraminifer *Globigerinoides ruber* from two marine sediment cores recovered in the Mozambique Channel off the Zambezi River, southwestern tropical Indian Ocean, reveal climate variability over the last 17 kyr. Analysis of samples collected from the water column of the Mozambique Channel validates that Mg/Ca in *Globigerinoides ruber* reflects calcification temperatures at 0-30 m water depth and that the surface water of the southwestern Indian Ocean is very sensitive to dissolved Ba input from adjacent rivers. Foraminiferal Ba/Ca and Mg/Ca time series are used to reconstruct hydrological and thermal changes over southeastern African and southwestern tropical ocean. The Mg/Ca-based sea surface temperature (SST) estimates indicate that the thermal evolution of the tropical southwestern Indian Ocean followed, within age model uncertainties, climate changes over Antarctica. The trend of the SST record is marked by a gradual warming from 24.7 ±0.6 °C at 17.0±0.2 kyr BP to 26.4 ±0.3 °C at 10-11 kyr BP interrupted by two prominent coolings of ~1.5 ±0.2 °C and ~1 °C centered at 15±0.1 kyr BP and 13.4±0.2 kyr BP, respectively. Declining SSTs in the early Holocene reach their minimum (25°C) at 8.7±0.2 kyr BP and give way to stable thermal conditions over the Middle and Late Holocene. The Ba/Ca record indicates that the Zambezi basin experienced relatively wet conditions during the early phase of the last deglaciation, Bølling-Allerød, and the early Holocene. These wet phases coincide with an increase of SST in the Mozambique Channel. In contrast, relatively dry conditions throughout the middle and late Holocene epoch are accompanied by relatively cold Mozambique Channel surface water. These shifts likely reflect a response to meridional shifts of the austral westerlies and subtropical front. These hypothesized shifts would have modulated the advection of cold Southern Ocean water into the Mozambique Channel. Changes in SST in the Mozambique Channel, and possible resultant changes in the zonal gradient in the tropical Indian Ocean, in turn, had a strong impact on the precipitation over southeastern Africa.

1. Introduction

Climate projection in the Fourth Assessment Report of the Intergovernmental Panel on Climate Change predicts that in 2090-2099 the southeastern Africa monsoon precipitation will decline by up to 20% relative to that of 1980-1999 (Meehl et al., 2007). Precipitation changes of this magnitude will have severe impacts in an already vulnerable subsistence agro-economy. Instrumental data show that the tropical Indian Ocean sea surface is steadily warming since the 1950s, amounting to an SST increase of 0.5 °C over the last 60 years (Du and Xie, 2008), and model studies identify links between southeastern African monsoon precipitation and southwestern Indian Ocean sea surface temperature (Behera and Yamagata, 2001; Cook, 2000; Reason, 2001). The link is established via increased occurrence of the subtropical Indian Ocean Dipole (Behera and Yamagata, 2001; Cook, 2000; Reason, 2001). Uncertainty in the model estimates is, however, significant due to lack of validation data for long-term projection. Deciphering past rapid hydrological changes in southern Africa and their link to Indian Ocean sea surface temperature may harbor information that is valuable to help assess long-term future climate trend. Recently published climate records from southern-southeastern African lakes (Brown et al., 2007; Castañeda et al., 2009; Garcin et al., 2006; Johnson et al., 2011; Kristen et al., 2010; Stager et al., 2011; Thomas et al., 2009) and marine sediments (Dupont et al., 2011; Schefuß et al., 2011; Wang et al., 2013a) reveal that southeastern African climate underwent rapid reorganization in response to high latitude ice sheet instabilities and large-scale atmospheric-oceanic circulation changes. However, conflicting proxy signals in the same marine sedimentary archive, such as the co-occurrence of proxies indicating enhanced precipitation and dominance of drought resistant plants (Schefuß et al., 2011), demonstrate the need for further paleo-hydrological studies. This study focuses on marine sediments recovered off the Zambezi River and presents Ba/Ca-based estimate of runoff changes and the first highly resolved Mg/Ca-SST record that provides a point of comparison for the organic based SST reconstruction published previously (Schefuß et al., 2011). Our results highlight the role of southern high latitude climate in shaping the SST of the southwestern Indian Ocean and the southeastern African hydrological evolution during the last deglaciation and the Holocene.

2. Core location and setting

The Mozambique Channel is located between Madagascar and Mozambique (Figure 1) and serves as conduit for southward transport of warm water masses originating from the equatorial and tropical Indian Ocean (Ridderinkhof et al., 2010; Schott et al., 2002; van der Werf et al., 2010). Surface circulation in the Mozambique Channel is dominated by eddies with annual net southward through flow of 16.7±3.1 Sv (1 Sv=10^6 m^3/s) (Ridderinkhof et al., 2010). Seasonal (4.1 Sv) and interannual (8.9 Sv) variability of the southward through flow and eddy formation in the Mozambique Channel is attributed to variability in the wind field in the western Indian Ocean and Indian Ocean Dipole Mode, respectively (Ridderinkhof et al., 2010; Schott et al., 2002; van der Werf et al., 2010). Frequent and strong eddy formation occurs in austral winter, causing relatively deep mixed layer (~45 m), relatively low sea surface temperature (SST), and high sea surface salinity (SSS) (Fallet et al., 2010; Ridderinkhof et al., 2010; van der Werf et al., 2010). Annual mean SST and SSS off the Zambezi Rivers are 26.5 °C and 35.1 practical salinity scale (psu), respectively (Antonov et al., 2010; Locarnini et al., 2010). Seasonal contrast in SST (SSS) is 3.5 °C (0.9 psu) with an average summer (January-March) SST of 28.8 °C (34.98 psu) and winter (July-September) SST of 25.24 (35.91 psu) (Antonov et al., 2010; Locarnini et al., 2010). Locally, as it will be shown below, SSS in the Mozambique Channel is strongly influenced by runoff from the Mahajanga and Betsiboka rivers (Madagascar) and the Zambezi River in southeastern Africa (Figures 1 and 2).

The Zambezi River is the largest river in southeastern Africa and drains an area of 1.39 million km^2 (Beilfuss and Santos, 2001). On decadal time scale, runoff of the Zambezi River is highly variable with an average value of 107±84 km^3/year. The large fluctuation (±84 km^3/year) in the average discharge estimates reflects decadal variability of monsoon precipitation (Beilfuss and Santos, 2001). Rainfall over the entire Zambezi basin and northeastern Madagascar is concentrated between November and March (southern hemisphere monsoon), with a peak in February and March (240-420 mm/month), and is linked to the seasonal movement of ITCZ that forms at the convergence of three distinct air masses: the southeast Trade Winds from the Indian

Ocean, the Congo Air from the west coast of Africa, and the northeast monsoon winds from the East African coast (Beilfuss and Santos, 2001). The seasonal runoff of Zambezi River varies strongly with 7000 m^3/sec during the height of rainfall season and 2000 m^3/sec during dry season (Beilfuss and Santos, 2001). The runoff shows also a strong interannual and decadal variability (Beilfuss and Santos, 2001), and as it enters the Mozambique Channel the runoff leaves a strong imprint in the sea surface salinity and trace element composition of seawater (Figure 2). The sediment load of the Zambezi River associated with runoff is estimated ~$20*10^6$ metric tons per year (Milliman and Meade, 1983) and results in high accumulation rate in the inner and outer shelf (Schulz et al., 2011). In this study, we focus on runoff and SST proxies from sediment sequences retrieved off the Zambezi River, with the aim of providing a high-resolution record of spatially integrated precipitation over Zambezi basin and its possible link to SST evolution in the southwestern Indian Ocean.

3. Methods

We analyzed Ba/Ca and Mg/Ca composition of seawater and planktonic foraminifera collected from water column and marine sediment cores that were retrieved off the Zambezi River and Madagascar Channel, southwestern Indian Ocean (Figure 1). During Meteor-cruise 75-3, we collected seawater from the sea surface to a water depth of 75 m and measured temperature and salinity along vertical profiles using a Conductivity-Density-Temperature (CDT)/Rosette sampler. The seawater samples and CDT data were collected during the rainy season and high runoff of the Zambezi, Mahajanga, and Betsiboka rivers (between February 29th and March 9th, 2008). Once the water sampler was on deck, water samples were immediately transferred into acid leached polyethylene containers (20 liters) and filtered using high performance pump and filter mesh of 0.45 µm (nitrocellulose). After filtration, water samples were acidified to pH ~2 using ultrapure hydrochloric acid (HCl) and stored in acid leached high density polyethylene 250 ml bottles. Ba concentration, reported in nmol/kg (Figure 2A) in seawater were analyzed by the isotope dilution/internal standard method described by

Lea and Spero (1994) using a Thermo Finnigan Element2 sector field ICP-MS. Analytical uncertainty of seawater Ba is ±2.9% (1σ).

A Multiple Opening/Closing Net (mesh width ≤ 63 µm) equipped with an Environmental Sensing System (MOCENSS) was used to collect planktonic foraminifers from water column depths between 5m to 400 m below the sea surface. Planktonic foraminifers were identified under the microscope and selected on board the research vessel. For trace element analysis, only living plankton foraminifers (at time of collection) were selected. To remove organic matter attached to foraminifer chamber walls, foraminifer tests were cleaned with NaOH-buffered 3% H_2O_2 in boiling water bath for 30 minutes. Following the approach described by Pak et al. (2004), test size of individual foraminifers was determined using ocular micrometer and chambers were opened using a scalpel for effective physical and chemical removal of remaining traces of organic tissue. Samples were transferred into acid leached vials and cleaned with NaOH-buffered 3% H_2O_2 in a boiling water bath for 30 minutes. This step was repeated two times. After oxidation, samples were rinsed several times with ultrapure water. Dissolved samples were analyzed by the isotope dilution/internal standard method described by Martin and Lea (2002) using a Thermo Finnigan Element2 sector field ICP-MS. Analytical reproducibility of Mg/Ca and Ba/Ca, assessed by analyzing consistency standards matched in concentration to dissolved foraminifera solutions and analyzed in the course of the entire study, is estimated at ±0.6% and ±1.8% (1σ), respectively.

Analysis of Mg/Ca and Ba/Ca of *Globigerinoides ruber* (*sensus strictus*) tests was carried out in samples from cores GeoB9307-3 (18°33.90'S, 37°22.80'E, water depth 542 m) and GeoB9310-4 (19°12.11'S, 37°02.49'E, water depth 543 m) that were recovered off the Zambezi River (Figure 1) 25-30 individuals of *G. ruber* were picked from the 250-300 µm size fraction for each analysis. Shells were gently crushed and cleaned using the UCSB standard foraminifera cleaning procedure (Martin and Lea, 2002) and as described above. We also analyzed Al/Ca, Fe/Ca, Mn/Ca and REE/Ca and used them as diagnostic tools to assess the success of the cleaning and a possible diagenetic imprint. Pooled standard deviation of duplicate analyses is ±0.08 mmol/mol for Mg/Ca and ±0.06 µmol/mol for Ba/Ca (n=147), which are larger than the SD of the analytical method.

Mg/Ca was converted to SST using the global equation: Mg/Ca (mmol/mol)=0.38*exp[0.09*T(˚C)] (Anand et al., 2003; Dekens et al., 2002). Given the shallow depth and excellent visual preservation of tests, we did not apply any dissolution correction.

We analyzed the $\delta^{18}O$ composition of G. ruber in GeoB9307-3 and GeoB9310-4. The analysis was carried out using an Isoprime IRMS at UCSB in 2007. The $\delta^{18}O$ data are reported on the PDB scale. The precision of $\delta^{18}O$ analysis was determined by analyzing NBS 19 standards and is estimated at ±0.07‰ (2σ). Using the Mg/Ca-based calcification temperature estimate, the temperature – $\delta^{18}O_{calcite}$ – $\delta^{18}O_{seawater}$ equation (Bemis et al., 1998), and estimate of $\delta^{18}O_{seawater}$ related to secular changes in the ice volume (Waelbroeck et al., 2002), we established a record of temperature and ice volume corrected $\delta^{18}O$ ($\delta^{18}O_{temp\text{-}ivc}$) time series. The cumulative error estimate of the $\delta^{18}O_{temp\text{-}ivc}$ values is ±0.32‰ (1σ).

The age models for marine sediment cores GeoB9307-3 and GeoB9310-4 are based on 32 ^{14}C-dating of monospecific and mixed foraminiferal tests (Table 1). Radiocarbon data were analyzed at the Leibniz-Laboratory for Radiometric Dating and Isotope Research in Kiel (Germany) and ^{14}C-ages were converted to calendar ages using calibration software CALIB (version 6.10) (Stuiver and Braziunas, 1993) and Marine09 data set (Reimer et al., 2009). We applied a constant reservoir age correction of ΔR= 203±32 for the southwestern Indian Ocean (Southon et al., 2002). The final age models are based on fourth order polynomial fits (Figure 3). According to the two age models, sample resolution varies between 40 and 90 years. All data are available in the first author's web site and the NOAA Paleoclimatology Data Center.

4. Results

4.1 Water column samples

There is a strong inverse relationship between dissolved Ba (nmol/kg) and seawater salinity in the Mozambique Channel (r^2=0.74, n=42) (Figure 2A). In the study

area, a large gradient in sea surface salinity occurs due to runoff from the Zambezi, Limpopo, Mahajanga, and Betsiboka rivers (Figures 1 and 2). To our knowledge, there is no available measurement of dissolved Ba from riverine water before it enters into the Mozambique Channel. While estuarine desorption and submarine groundwater may contribute to the elevated Ba off the Zambezi River, as suggested for other large river systems (Moore, 1997), the enrichment of dissolved Ba off the Zambezi River and Madagascan rivers is largely related to a high concentration of Ba in the runoff, as demonstrated in other low latitude river systems (Carroll et al., 1993; Edmond et al., 1978; Moore, 1997; Singh et al., 2013). Based on the dissolved Ba-salinity relationship (Figure 2A), we estimate an effective end member (including estuarine desorption and submarine groundwater discharges) for riverine Ba concentration of 395±64 nmol/kg. This value is approximately eleven-fold higher than the Ba content (37±5 nmol/kg) of Mozambique Channel seawater with minimal fresh water influence. The latter is comparable to open-ocean Indian Ocean surface values of ~35 nmol/kg (Monnin et al., 1999). Our estimate of dissolve Ba concentration in Zambezi River water, based on the end member calculation, is close to the average value analyzed in water of the Mississippi River (~465 nmol/kg) and approximately three-fold higher than found for the Congo River (~130 nmol/kg) (Edmond et al., 1978). The comparison of Ba in Mozambique Channel surface water with Ba analyzed off other large river systems reveals that although the geology of the catchment, weathering of the soil, and vegetation cover plays an important role, the amount of runoff is the most dominant factor in determining dissolved Ba (Figure S1 in the supplemental material). In summary, our findings indicate that Ba in seawater of the Mozambique Channel is a sensitive indicator of riverine runoff. Because Ba uptake in planktonic foraminifer calcite linearly correlates to Ba concentration in seawater (Hönisch et al., 2011; Lea and Spero, 1994), Ba/Ca in tests of *G. ruber*, a low salinity-tolerating species (Ufkes et al., 1998), is a powerful proxy to independently reconstruct past variation of runoff and, hence, indirectly, the precipitation history over river basins (Weldeab, 2012; Weldeab et al., 2007a; Weldeab et al., 2007b).

As a test of how well foraminiferal Mg/Ca records regional SST, we analyzed Mg/Ca in *G. ruber* tests collected from the water column by MOCNESS tows (Figure 2B

and Table 2). Though the data set is too small to allow in-depth analysis, there is no systematic relationship between sampling depth and Mg/Ca values, indicating that *G. ruber* tests collected at deeper water depths originate from shallow depths. Figure 2B shows Mg/Ca data plotted versus average temperature (0-30 meter) obtained via CDT measurements at the location and time of foraminifer sampling (between February 29th and March 9th, 2008). The sea surface salinity at the sampling sites is below 35.5 psu, therefore a strong salinity influence on the Mg/Ca data is not expected. The Mg/Ca-temperature estimates plot within the global calibration curve (Mg/Ca = 0.038 (±0.02)x exp(0.09 (±0.003)xT) (Anand et al., 2003; Dekens et al., 2002). Our Mg/Ca data (4.66±0.47, n=6) are consistently lower than those (5.53 ±0.47, n=7) collected in February-March between 2004 and 2006 and analyzed in *G. ruber* (250-315 µm) from a sediment trap time series in the Mozambique Channel (Fallet et al., 2010). This deviation can be attributed to differences in test size and the influence of interannual variability, as evident in the sediment trap time series collected between 2003 and 2006 (Fallet et al., 2010).

4.2 Down core time series

4.2.1 Sediment deposition

Sediment cores GeoB9307-3 and GeoB9310-4 provided a continuous sediment accumulation over the last 17 and 14 thousand years before present (kyr, BP), respectively (Figure 3A). Sediment deposition rate was highest during the late deglacial and early Holocene, with peak values of ~130 cm/kyr at ~12 kyr BP and an average value of 80±25 cm/kyr between 11 and 17 kyr BP in GeoB9307-3 (Figure 3B). Holocene deposition rates were significantly lower and markedly different between the two sites, with relatively higher rates at GeoB9310-4 (39±16 cm/kyr) than at GeoB9307-3 (18±6 cm/kyr) site. Figure 3B illustrates that a spatial shift of the deposition center occurred during the deglacial and early Holocene. Changes in the amount of riverine sediment delivery and lateral shifts of deposition centers off the Zambezi River can be linked to a multitude of processes such as channel avulsion, which arises as a result of the interplay

between changes in riverine discharge rate and along-shore wave-induced net sediment drift (Bhattacharya and Giosan, 2003), sea-level changes, and changes in channelized sediment transport (Beiersdorf et al., 1980; Schulz et al., 2011; Ulrich and Pasenau, 1973). The area off the Zambezi River has been studied in detail, including high-resolution bathymetric mapping (Ulrich and Pasenau, 1973), seismic profiling (Beiersdorf et al., 1980), and a spatio-temporal investigation of sediment composition (Schulz et al., 2011). A finding that is of particular interest for our study is the discovery of the 185 m deep Chinde-Zambezi paleo-Channel that was filled during the last deglacial sea-level rise (Beiersdorf et al., 1980). The east-west orientation of the paleo-channel, its proximity to GeoB9307-3 site, and the timing of inactivation via filling are fully consistent with the evolution of the sedimentation rate at GeoB9307-3 site (Figure 3B). We note, as elaborated below, that the timing of highest sedimentation rate and subsequent decline coincides with elevated Zambezi runoff, suggesting that not only sea-level rise (Beiersdorf et al., 1980) but also enhanced riverine sediment delivery may account for the fill and inactivation of the channel that most likely led to defocusing and shift of sediment delivery.

4.2.2, Mg/Ca, Ba/Ca, and $\delta^{18}O$ time series

For each proxy parameter, we create a binned composite record (bin size 220 yr) of time-series analyzed in core GeoB9310-4 and GeoB9307-3 (Figure 4). The binned composite record covers the time window between 0.1 and 14 kyr cal BP. Record older than 14 kyr cal BP is based on the un-binned time-series analyzed in GeoB9307-3. Our discussion focuses on the binned composite (0.1 and 14 kyr cal BP) and un-binned (14-17.3 kyr cal BP) records.

Variations in Mg/Ca from tests of the mixed layer-dwelling foraminifera *G. ruber* provide a quantitative estimate of past SST changes in the southwestern Indian Ocean. The multi-decadal scale deglacial record is marked by large fluctuations in Mg/Ca (Figure 4). Due to age model uncertainty at multi-decadal scale, we focus on multi-centennial and millennial time scale variation. On multi-millennial time scales, the

evolution of deglacial SSTs indicates a warming trend from 24.7±0.6 °C between 17 and 15.5 kyr BP to 26.5±0.4 °C between 11 and 10 kyr BP (Figure 4). Two prominent coolings of ~1.2 °C and ~1 °C magnitude are evident, centered between 15.5 and 14.7 kyr BP and 13.5 and 12.7 kyr BP, respectively. At ~13 kyr BP, a gradual warming resumes and reaches a plateau of 26.5±0.3 °C at 11 kyr BP, which persisted until 10 kyr BP. Declining SSTs in the early Holocene reach their minimum (24.9 °C) at 8.7±0.2 kyr BP and give way to relatively stable thermal conditions over the Middle and Late Holocene, with an average SST of 25.5±0.3 °C (8.6-3 kyr BP). The core top SST value of 26.2 °C (0.4 kyr BP) is very similar to the modern annual average SST of 26.4˚C (Locarnini et al., 2010).

The Ba/Ca time series varies between 0.69 and 1.35 µmol/mol. For reference, typical open ocean Ba/Ca values for surface-dwelling foraminifera are 0.7±0.1 µmol/mol (Lea and Boyle, 1991). In core GeoB9310-4, Ba/Ca shows a significant correlation with an r^2 of 0.53 and p-value of << 0.0001 (n=200) with Mn/Ca, which varies between 15 and 117 µmol/mol (Figure S3). The correlation likely indicates a diagenetic imprint that may explain the slightly elevated deglacial Ba/Ca values in GeoB9310-4 relative to those of GeoB9307-3 (Figure S3). The correlation in core GeoB9307-3 between Ba/Ca and Mn/Ca – which varies between 13 and 118 µmol/mol -- is less robust but still highly significant, with an r^2 value of 0.19 (n=185) and p-value << 0.0001 (Figure S3). We corrected the Ba/Ca time series for the likely diagenetic overprinting using the following equations:

$$Ba/Ca_{corrected} = Ba/Ca_{analyzed} - 0.0077*(Mn/Ca - 15) \text{ for GeoB9310-4}$$

$$Ba/Ca_{corrected} = Ba/Ca_{analyzed} - 0.0036*(Mn/Ca - 15) \text{ for GeoB9307-3}$$

The value of 15 is the lowest Mn/Ca value analyzed and likely represents the Mn/Ca content of pure foraminiferal calcite at this site. We note that the uncorrected and corrected Ba/Ca values in GeoB9307-3 differ only slightly (Figure S3).

On millennial timescales, the corrected Ba/Ca in both cores GeoB9310-4 and GeoB9307-3 shows a comparable magnitude and follow the same trend (Figure 4d). Starting from the early deglacial, Ba/Ca declines from 1.35 to 0.78 µmol/mol at 14.9 kyr.

Between 14.9 and 13.4 kyr, Ba/Ca shows elevated values followed by a time window (13.4- 11.3 kyr) of low Ba/Ca and high frequency variation. The interval spanning the early and middle Holocene is marked by a gradual rise, prolonged plateau value, and gradual decline of Ba/Ca values. Between 7 and 0.4 kyr, Ba/Ca is low, varying between 0.8 and 0.65 μmol/mol with an interruption by an interval of elevated Ba/Ca between 2.45 and 1.5 kyr.

The Holocene $\delta^{18}O$ record analyzed in *G. ruber* shows two remarkably stable trends between 0.1 and 5.5 kyr and 5.75 and 8.7 kyr BP with an average value of -2.05±0.08 ‰ (n=29) and -1.97±0.06 ‰ (n=36) (Figure 4a). From the early deglacial (16.4 - 17.3 kyr) to the early Holocene (8.73 - 11 kyr), the $\delta^{18}O$ values gradually shifted from -0.66±0.09 ‰ (n=6) to -1.7±0.12 ‰ (n=34).

5 Discussions

5.1 SST trend and its link to Antarctic climate

The high resolution SST record from the two cores provides unprecedented detail that extends observations from other records from the southwestern tropical Indian Ocean (Bard et al., 1997; Caley et al., 2011; Kiefer et al., 2006; Levi et al., 2007; Wang et al., 2013b). Interestingly, a comparison of the Mg/Ca- (this study) and TEX_{86}-based SST estimates in core GeoB9307-3 (Schefuß et al. 2011) – one of the same cores utilized in this study – reveals a stark contrast during the deglacial (Figure 5). The deviation between the two SST proxies can be caused by several factors, including changes in depth habitat, seasonality, calibration, and influence of terrestrial input. We note a close correspondence in the variability of terrestrial organic matter (TOM), as indicated by the branched isoprenoid tetraether (BIT)-index, and the TEX_{86}-derived SST record (Figure 5). At times of significantly elevated input of TOM, the TEX_{86}-derived SST is higher by up to ~3 °C when compared to Mg/Ca-based SST. Throughout the Holocene where the input of TOM was very low, the comparison reveals better agreement of TEX_{86}-derived and Mg/Ca-based SST estimates (Figure 5). On the basis of marine core-top and soil sample analyses and end-member modeling, Weijers et al (2006) demonstrated that an

elevated input of TOM (high BIT-index) exerts a substantial bias in TEX_{86}-derived SST estimates. Similarly, Powers et al. (2010) conclude that an enhanced supply of soil-derived organic matter to lake sediments leads to an overestimate of TEX_{86}-derived surface temperature. Weijers et al. (2006) show that a BIT-index of 0.4 leads to an overestimate of SST by more than 2 °C. While changes in habitat depth and seasonality of both *G. ruber* and Crenarchaeota might had contributed to the SST divergence in the same core material, according to the findings of Weijers et al. (2006) the elevated deglacial and early Holocene BIT index (0.4-0.77, average: 0.54±0.11; n=68) may suggest a significant terrestrial influence on the TEX_{86} ratio and resultant SST estimate.

The Mg/Ca-based SST record from the Mozambique Channel cores indicates that the evolution of southwestern tropical Indian Ocean SST follows an Antarctic climate pacing (Figure 6). Taking age model uncertainty into consideration that in part may arise due to the assumption of constant reservoir age and can be up to ±650 years, a drop of 1.2˚C in the Mozambique Channel SST record between 13.5 and 12.5 kyr aligns with the colder interval of the Antarctic Cold Reversal (ACR) in the Dronning Maud Land (EDML) ice core record (Parrenin et al., 2013) (Figure 6). Similarly, an SST decrease of ~1˚C parallels and overlaps with a break of the general warming trend of Antarctic climate between 15.6 and 14.7 kyr BP (EPICA-Community-members, 2006; Parrenin et al., 2013). The millennial-scale temperature trend of the Mozambique Channel record between 12.5 and 8 kyr BP also shares several commonalities with Antarctica ice core records (Figure 6). We suggest that this temporal correlation indicates a thermal link between the southwestern tropical Indian Ocean and the southern high latitudes. Last deglacial thermal evolution in the southern high latitude is thought to relate to changes in the strength of Atlantic meridional overturning circulation, southern high latitude warming and southward shift of the austral westerlies, and global warming driven by rising atmospheric CO_2 (Anderson et al., 2009; EPICA-Community-members, 2006; Shakun et al., 2012; Toggweiler and Lea, 2011). Modern observation shows a strong link between Southern Ocean warming, poleward shift of the austral westerlies, and increased leakages of warm and saline Indian Ocean water into the southern Atlantic Ocean (Alory et al., 2007; Beal et al., 2011; Biastoch et al., 2008; Biastoch et al., 2009). In response to an intensification and southward shift of the austral westerlies and subtropical front,

surface and subsurface warming is observed across the subtropical Indian Ocean, with stronger and deeper warming in the western Indian Ocean relative the eastern part the Indian Ocean (Alroy, et al. 2007). We suggest that the poleward retreat of the westerlies and the sub-tropical front during the deglacial (Anderson et al., 2009) reduced the advection of cold Southern Ocean water into the Mozambique Channel and contributed to the SST rise.

Alternatively, changes in the strength and rate of eddy formation in the northern Mozambique Channel may have played a significant role in shaping SST evolution in the Mozambique Channel. Under modern conditions, during austral winter enhanced eddy formation occurs in response to changes in wind field in the western Indian Ocean, thereby deepening the mixed layer and lowering the SST in the Mozambique Channel (Ridderinkhof et al., 2010; van der Werf et al., 2010). On interannual timescales, the variability of eddy formation is attributed to the Indian Ocean Dipole Mode (Ridderinkhof et al., 2010). Analogous to modern observations (Behera and Yamagata, 2001; Reason, 2001), a relatively weak zonal temperature gradient between the western and eastern subtropical Indian Ocean during the distinct intervals within the deglacial and early Holocene (Figures, 7 and 8), may indicate that changes in the thermal structure and wind patterns across the tropical Indian Ocean reduced the strength and rate of eddy formation in the Mozambique Channel. Changes in the reconstructed IO zonal gradient, however, mainly arise from SST changes in the Mozambique Channel site (Figure 6). Therefore, while we do not rule out that decreased eddy formation was a contributing factor to surface warming, we hypothesize that the SST record most likely reflects a response to reduced advection of Southern Ocean cold water into the Mozambique Channel, which occurred in response to a southward shift of the austral Westerlies. The latter might be related to interhemispheric climate oscillations. In summery, the Mg/Ca SST record highlights a strong control of large-scale atmospheric and oceanic changes in the southern high latitude on the thermal state of the southwestern tropical Indian Ocean.

5.2 Zambezi runoff and precipitation over Southeastern Africa

We utilize Ba/Ca in tests of *G. ruber* as a proxy for changes in riverine discharge of the Zambezi River. Our analysis of surface water shows that runoff of the Zambezi

River and Madagascan rivers exerts the dominant control on the Ba composition of seawater over the core site (Figures 2A). Past variability of Ba composition of seawater and, hence runoff variability, can be reconstructed using Ba/Ca in calcite test of surface dwelling planktonic foraminifer *G. ruber* (Hall and Chan, 2004; Lea and Boyle, 1991; Weldeab, 2012; Weldeab et al., 2007a; Weldeab et al., 2007b). A direct calibration between Ba in Mozambique Channel seawater and *G. ruber* Ba/Ca was not possible because of the small MOCNESS sample sizes. Culture experiments, however, demonstrate that Ba-uptake in planktonic foraminifer is linearly correlated to Ba in seawater in which the foraminifers calcify (Hönisch et al., 2011; Lea and Spero, 1994).

Before discussing Ba/Ca as an indicator of changes in the amount of runoff, we consider the hypothesis that changes in Ba/Ca are significantly correlated with episodes of rapid global sea level rise, changes in sediment delivery, and redirection of sediment load route. The relatively high Ba/Ca during the early deglacial (17.3 -16 kyr) and the drop in Ba/Ca between 16 and 14.7 kyr correspond to a relatively slow rate and rapid sea level rise (Clark et al., 2009; Deschamps et al., 2012; Waelbroeck et al., 2002), respectively (Figure 7). Relatively high Ba/Ca between 14.7 and 13.5 kyr cal BP overlaps with very rapid (14.7-14.3 kyr BP) (Deschamps et al., 2012) and relatively moderate rate of sea level rise (14.3-13.5 kyr BP) (Clark et al., 2009; Deschamps et al., 2012; Waelbroeck et al., 2002). Furthermore, at times of continuous sea level rise Ba/Ca is declining (13.5 - 11.1 kyr BP). Between 8 kyr BP and the core top (0.1 kyr BP) (Fig. 6A), the Ba/Ca time series shows relatively low values with an average value of 0.79±0.08 µmol/mol (n=40). We cannot exclude the possibility that sea level changes contributed to the orbital-scale Ba/Ca trend; however, the observation that Ba/Ca has similar levels between 16 and 14.6 kyr cal BP and again between10 and 8 kyr cal BP, despite a sea level increase of ~ 90-100 m from 16 to 8 kyr, suggests that sea level changes are not the dominant factor that shapes the overall trend of the Ba/Ca record. In addition, the lack of a strict correspondence between the Ba/Ca record and global sea level changes indicates that millennial scale changes in Ba/Ca are not controlled by changes in sea level (Figure 7).

The peak in bulk sediment accumulation rate occurs between 13 and 11 kyr BP in core GeoB9307-3 and between 12.5 and 9 kyr BP in core GeoB9310-4 (Figure 3). The effect of high accumulation of bulk sediment on dissolved Ba in the Mozambique Channel appears to be limited, as suggested by the following observations: 1) whereas the timing of high bulk sediment accumulation rate between GeoB9310-4 and GeoB9307-3 is markedly different, the trend and magnitude of the corrected Ba/Ca records in both GeoB9310-4 and GeoB9307-3 are indistinguishable within the uncertainty of sample reproducibility (Figure 4). The high accumulation rate of bulk sediment in GeoB9307-3 between 13 and 11 kyr BP is accompanied by declining and low Ba/Ca, and the highest sediment accumulation rate in GeoB9310-4 does not coincide with high Ba/Ca. Although lower sea level reduces the distance between the core sites and the Zambezi River mouth, the above-described observations indicate that the increase of dissolved Ba and its manifestation in *G. ruber* test is mainly due to the increase of runoff. The lack of correlation between Mg/Ca-SST estimates and Ba/Ca may indicate that upwelling of cold water is most likely not responsible for changes in the Ba/Ca record. Whether the increase of runoff is related to increase of precipitation over a certain segment of the Zambezi River catchment or reflect a basin-wide changes cannot be determined in this study.

The strongest correlation between the $\delta^{18}O_{temp\text{-}ivc}$ and Ba/Ca records occur between 13.5 and 8 kyr (Fig. 8). A close look reveals a deviation in the timing of the onset and termination of freshening and increased runoff, as indicated by $\delta^{18}O_{temp\text{-}ivc}$ and Ba/Ca, respectively. For example, the Ba/Ca and the $\delta^{18}O_{temp\text{-}ivc}$ indicate a rise in runoff and lower salinity during the Bølling-Allerød chronozone. The timing of the onset (14.7 kyr BP) and termination (13.5 kyr BP) of the wet phase in the Ba/Ca record, however, differs from the $\delta^{18}O_{temp\text{-}ivc}$ record, whose onset and termination is centered at 15.5 and 13 kyr BP, respectively (Figure 8). In contrast, the declining Ba/Ca trend during the middle Holocene is not reflected in the $\delta^{18}O_{temp\text{-}ivc}$ record, and the slightly depleted $\delta^{18}O_{temp\text{-}ivc}$ values between 5.5 and 2.5 kyr is not evident in the Ba/Ca record. Similarly, the relatively high Ba/Ca values during the early deglacial are not accompanied by a strong depletion in the $\delta^{18}O_{temp\text{-}ivc}$ record. A possible explanation for the deviations of the

$\delta^{18}O_{temp\text{-}ivc}$ record from the Ba/Ca record, as well as other regional climate records, is a shift in the isotope composition of precipitation and seawater. Such shifts have been observed before in paleo-records (Rohling et al., 2009; Saraswat et al., 2013; Weldeab, 2012; Weldeab et al., 2007a). Modeling studies indicate that changes in the evapo-precipitation balances and sources and sinks of moisture can lead to $\delta^{18}O$ shifts in precipitation (LeGrande and Schmidt, 2009; LeGrande et al., 2006; Pausata et al., 2011). The relatively wet climate during the deglacial, as suggested by the Ba/Ca record, is clearly supported by several paleoclimate records from the region, as discussed below.

Deglacial humid conditions in the Zambezi basin, as inferred from the Ba/Ca record, are consistent with reconstructed high-stands of Lake Malawi (Filippi and Talbot, 2005; Johnson et al., 2002), Lake Chilwa (Thomas et al., 2009), and Lake Tritrivakely (Williamson et al., 1998). In line with our observation, biomarker time series from Lake Malawi sediment sequence (Castañeda et al., 2009) suggests relatively humid conditions between 17 kyr BP and 13.6 kyr BP. Farther to the south of the Zambezi basin, most recent records from Lake Tswaing (Northeastern South Africa) (Kristen et al., 2007; Kristen et al., 2010; Partridge et al., 1997) and re-interpretation of the stalagmite record from the Magapansgat Valley (Holmgren et al., 2003; Lee-Thorp et al., 2001; Scott et al., 2008; Scott et al., 2012) suggest that the onset of relatively wet conditions was centered at ~17.5 kyr BP. For more detailed information, we compare the Ba/Ca record with a lake level reconstruction of Lake Chilwa (Thomas et al., 2009) and pollen records from Lake Tritrivakely (Williamson et al., 1998) and Wonderkrater in South Africa (Scott et al., 2012) (Figure 8). We note that temperature imprint in the pollen records may explain some of the trend (Williamson et al, 1998, Scott et al., 2012). It is, however, difficult to disentangle the temperature effect from the moisture effect. Lake Chilwa is located in the northeastern periphery of the Zambezi catchment, Lake Tritrivakley in the high land of central Madagascar, and Wonderkrater lies ~ 500 km south of the southern margin of the Zambezi basin (Figure 1). Figure 8 highlights the consistency between the deglacial Ba/Ca record and other regional the records (Thomas et al., 2009, Williamson et al, 1998, Scott et al., 2012). On sub-orbital scale, all four records indicate a relatively wet deglacial and dry Holocene (Figure 8). Although the centennial-to-millennial scale age model uncertainties of the Mozambique Channel and Chilwa records do not allow confident

point-point comparison, two prominent Ba/Ca peaks centered at 17.3-16 and 14.6-13.6 kyr BP, indicating episodes of elevated riverine discharge, do overlap with the timing of Lake Chilwa high-stands (Thomas et al., 2009). We note that these short-term wet episodes fall within the first half of Heinrich event 1 (H1), as defined by Stanford et al. (2011), and the Bølling-Allerød. The decline of Ba/Ca at 13.5 kyr BP predates the onset of the Younger Dryas by 600 years, likely within age model error. Starting at 11.1 kyr BP, the Ba/Ca record suggests gradually increased runoff, before runoff started to decline at 8.7 kyr BP.

Overall, on sub-orbital time scales, a consistent picture emerges indicating that southeastern Africa experienced relatively wet conditions during the last deglacial and early Holocene. In contrast to the pollen record from Wonderkrater in South Africa (Scott et al., 2012, Metwally et al., 2014, Truc et al., 20013), the Mozambique Channel middle and late Holocene Ba/Ca record shows persistently low values, indicating limited riverine runoff reaching the core site and weak precipitation in the Zambezi catchment. A possible explanation for the divergent trend between the Mozambique Channel and the Wonderkrater pollen records (Scott et al., 2012) is that the Wonderkrater is relatively far from the Zambezi Basin and might be influenced by air masses originating from the south. Our Holocene record is consistent with low accumulation rates of Fe/Ca, soil organic matter, and an increase in drought resistant plants in the Zambezi catchment, as recorded in GeoB9307-3 material (Schefuß et al., 2011). The absence of a noticeable and temporally extended high-stand in Lake Chilwa and continuous decline of moist-indicating pollen time series from Lake Tritrivakely lend support to our interpretation of the middle and late Holocene. In summary, with the exception of middle and late Holocene wet conditions suggested by the Wonderkrater pollen record (Scott et al., 2012), our record is consistent with regional records, indicating a response to a common climate forcing.

5.3 Link between zonal Indian Ocean SST gradient and Precipitation

On orbital time scales, several African paleo-precipitation records show a strong link to changes in solar insolation at precessional time scales (deMenocal, 1995; Partridge et al., 1997; Trauth et al., 2003; Weldeab et al., 2007a). Although punctuated by millennial-scale changes, the decreasing trend of Ba/Ca from 17.3 to 12.5 kyr BP parallel to declining southern hemisphere summer insolation values may argue for a causal link (Figure 8). Increasing Ba/Ca and depleted $\delta^{18}O_{temp\text{-}ivc}$ between 11.2 and 9.2 kyr BP coincides with the lowest solar insolation over the region (Figure 8). Similarly, rising solar insolation during the middle and late Holocene (0-7 kyr BP) corresponds to low Ba/Ca and relatively stable $\delta^{18}O_{temp\text{-}ivc}$, suggesting that changes in solar insolation were not the primary control on Zambezi basin rainfall variability at that time (Figure 8). Similarly, the pollen record from Lake Tritrivaketly (Williamson et al., 1998) suggests a continuous decline of moisture availability throughout the middle and late Holocene (Figure 8). A possible decoupling between precession-driven insolation changes and southeastern Africa precipitation has been inferred in previous work (Scholz et al., 2007; Stager et al., 2011; Thomas et al., 2009), but a plausible explanation is still lacking.

To evaluate the potential impact of changing tropical SST patterns in the southern tropical Indian Ocean, we combine the Mozambique Channel SST record and an SST record from the eastern tropical Indian Ocean (Xu et al., 2008) to calculate temporal trends in the zonal gradient (Figures 1, 6 and 8). During the last deglaciation and early Holocene, the relatively wet episodes in the Zambezi basin, as suggested by enhanced Ba/Ca, are associated with a relatively weak zonal SST gradient (Figure 8). Conversely, reduced riverine discharge over the last 9 kyr BP corresponds to a significantly stronger gradient. We note that the decrease in the zonal gradient is mainly driven by SST changes in the western tropical Indian Ocean (Figures 6 and 8). We therefore cannot rule out that the precipitation changes over the Zambezi basin were responding mainly to regional SST changes. Modern observations emphasize, however, the importance of zonal SST gradients across the tropical Indian Ocean for precipitation over southeastern Africa. Analogous to the Indian Ocean Dipole (IOD) (Saji et al., 1999; Webster et al., 1999), at present a subtropical dipole occasionally develops when warm SST in the southwestern Indian Ocean and cold surface water in the southeastern Indian Ocean (off western Australia) prevails during austral summer (Behera and Yamagata, 2001; Reason, 2001).

This constellation of factors gives rise to incursions of moisture-laden southeasterly air masses and the development of strong convection over the warm southeastern African continent, which in turn gives rise to abundant rainfall. If modern observations can serve as an analogy to infer mechanism of past thermal and hydrological linkages, then it is likely that over the last 17 kyr BP changes in the zonal SST gradient contributed in shaping past southeastern African rainfall variability. This could have facilitated an enhanced occurrence of rainfall-favorable conditions over southeastern Africa. An interesting implication of our results lies in lending support to the notion that in a warming climate, as currently observe, the southward shift of austral westerlies may lead to additional surface warming of western subtropical Indian Ocean and associated changes in rainfall in south-eastern Africa.

5. Conclusion

We present a high-resolution Mg/Ca-based SST record from the Mozambique Channel, in the southwestern tropical Indian Ocean. Considering age model uncertainty, the timing of millennial-scale SST changes in the southwestern Indian Ocean follows changes in Antarctic climate, as recorded in the $\delta^{18}O$ record of Antarctic ice cores (Blunier and Brook, 2001; EPICA-Community-members, 2006). The most likely mechanism linking Antarctic climate changes to the southern tropical Indian Ocean is latitudinal shifts of the austral westerlies and the subtropical front. We hypothesize that a southward shift of the westerlies reduces the thermal influence in the Mozambique Channel water, most likely by weakening the advection of cold Southern Ocean water into the Mozambique Channel.

Seawater data from Mozambique Channel demonstrate that this region is highly sensitive to dissolved Ba in Zambezi River runoff. We interpret the *G. ruber* Ba/Ca time series from the Mozambique Channel sediment cores as an indirect measure of Zambezi runoff variability, which in turn reflects changes in precipitation over the riverine basin. We used the Ba/Ca time series to reconstruct past changes in runoff of the Zambezi River. The middle and late Holocene Ba/Ca record suggests low runoff and weak

monsoon precipitation. In contrast, the deglacial and early Holocene record reveals phases of relatively high Ba/Ca, indicating stronger monsoon precipitation. We hypothesize that the modulation of SST in the Mozambique Channel by latitudinal shifts of the austral westerlies and subtropical front and resultant changes in the zonal SST gradient of southern tropical Indian Ocean present a viable explanation for the relatively wet deglacial and early Holocene conditions in southeastern Africa.

6. Acknowledgements

We thank the crew and participants of Meteor cruise M63/1 and M75/3. We thank Georges Paradis for ICP-MS operation and Deborah Khider for help with data processing. We thank Rainer Zahn and Ian Hall for help with water and MOCNESS samplings during M75-3. This study was supported by Deutsche Forschungsgemeinschaft Postdoctoral Fellowship Grant WE 2686/2-1 to SW, NSF Grant No OCE 0602362 to DWL, and UCSB start-up support to SW. We thank Jürgen Pätzold for valuable comments on a previous version of the manuscript.

Cited References

Alory, G., Wijffels, S., Meyers, G., 2007. Observed temperature trends in the Indian Ocean over 1960-1999 and associated mechanisms. Geophys. Res. Lett. 34, L02606.

Anand, P., Elderfield, H., Conte, M.H., 2003. Calibration of Mg/Ca thermometry in planktonic foraminifera from a sediment trap time series. Paleoceanography 18, 1050.

Anderson, R.F., Ali, S., Bradtmiller, L.I., Nielsen, S.H.H., Fleisher, M.Q., Anderson, B.E., Burckle, L.H., 2009. Wind-Driven Upwelling in the Southern Ocean and the Deglacial Rise in Atmospheric CO2. Science 323, 1443-1448.

Antonov, J.I., D. Seidov, Boyer, T.P., Locarnini, R.A., Mishonov, A.V., Garcia, H.E., Baranova, O.K., Zweng, M.M., Johnson, D.R., 2010. World Ocean Atlas 2009, Volume 2: Salinity, In: Levitus, S. (Ed.), NOAA Atlas NESDIS 69. U.S. Government Printing Office, , Washington, D.C., p. 184 pp.

Bard, E., Rostek, F., Sonzogni, C., 1997. Interhemispheric synchrony of the last deglaciation inferred from alkenone palaeothermometry. Nature 385, 707-710.

Beal, L.M., De Ruijter, W.P.M., Biastoch, A., Zahn, R., 2011. On the role of the Agulhas system in ocean circulation and climate. Nature 472, 429-436.

Behera, S.K., Yamagata, T., 2001. Subtropical SST dipole events in the Southern Indian Ocean. Geophysical Research Letters 28, 327-330.

Beiersdorf, H., Kudrass, H.R., von Stackelberg, U., 1980. Placer deposits of illmenite and zircon on the Zambezi Shelf. Geologisches Jahrbuch D36, 5-85.

Beilfuss, R., Santos, D., 2001. Patterns of Hydrological Change in the Zambezi Delta, Mozambique (Working Paper No. 2, International Crane Foundation, Sofala, Mozambique, 2001); available at http://www.savingcranes.org/images/stories/ pdf/conservation/Zambezi_hydrology_Working_Paper2.pdf., pp. 1-89.

Bemis, B.E., Spero, H., Bijma, J., Lea, D.W., 1998. Reevaluation of oxygen isotope composition of planktonic foraminifera: experimental results and revised paleotemperature equations. Paleoceanography 13, 150-160.

Berger, A., Loutre, M.F., 1991. Insolation values for the climate of the last 10 million years. Quaternary Science Review 10, 297-317.

Bhattacharya, J.P., Giosan, L., 2003. Wave-influenced deltas: geomorphological implications for facies reconstruction. Sedimentology 50, 187-210.

Biastoch, A., Boning, C.W., Lutjeharms, J.R.E., 2008. Agulhas leakage dynamics affects decadal variability in Atlantic overturning circulation. Nature 456, 489-492.

Biastoch, A., Boning, C.W., Schwarzkopf, F.U., Lutjeharms, J.R.E., 2009. Increase in Agulhas leakage due to poleward shift of Southern Hemisphere westerlies. Nature 462, 495-498.

Blunier, T., Brook, E.J., 2001. Timing of millennial-scale climate change in Antarctica and Greenland during the last glacial period. Science 291, 109-112.

Brown, E.T., Johnson, T.C., Scholz, C.A., Cohen, A.S., King, J.W., 2007. Abrupt change in tropical African climate linked to the bipolar seesaw over the past 55,000 years. Geophysical Research Letters 34, L20702.

Caley, T., Kim, J.-H., Malaizé, B., Giraudeau, J., Laepple, T., Caillon, N., Charlier, K., Rebaubier, H., Rossignol, L., Castañeda, I.S., Schouten, S., Sinninghe Damsté, J.S., 2011. High-latitude obliquity as a dominant forcing in the Agulhas current system. Climate of the Past 7, 1285-1296.

Carroll, J., Falkner, k.K., Brown, E.T., Moore, W.S., 1993. The role of the Ganges-Brahmaputra mixing zone in supplying barium and 226Ra to the Bay of Bengal. Geochimica et Cosmochimica Acta 57, 2981-2990.

Castañeda, I.S., Werne, J.P., Johnson, T.C., Filley, T.R., 2009. Late Quaternary vegetation history of southeast Africa: The molecular isotopic record from Lake Malawi. Palaeogeography, Palaeoclimatology, Palaeoecology 275, 100-112.

Clark, P.U., Dyke, A.S., Shakun, J.D., Carlson, A.E., Clark, J., Wohlfarth, B., Mitrovica, J.X., Hostetler, S.W., McCabe, A.M., 2009. The Last Glacial Maximum. Science 325, 710-714.

Cook, K.H., 2000. The south Indian Ocean convergence zone and interannual rainfal l variability. Journal of Climate 13, 3789-3804.

Dekens, P.S., Lea, D.W., Pak, D.K., Spero, H.J., 2002. Core top calibration of Mg/Ca in tropical foraminifera: refining paleo-temperature estimation. Geochemistry Geophysics Geosystems 3, 1022, doi: 1010.1029/2001GC000200.

deMenocal, P.B., 1995. Plio-Pleistocene African climate. Science 270, 53-59.

Deschamps, P., Durand, N., Bard, E., Hamelin, B., Camoin, G., Thomas, A.L., Henderson, G.M., Okuno, J.i., Yokoyama, Y., 2012. Ice-sheet collapse and sea-level rise at the Bolling warming 14,600 years ago. Nature 483, 559-564.

Du, Y., Xie, S.-P., 2008. Role of atmospheric adjustments in the tropical Indian Ocean warming during the 20th century in climate models. Geophys. Res. Lett. 35, L08712.

Dupont, L.M., Caley, T., Kim, J.-H., Castañeda, I., Malaizé, B., Giraudeau, J., 2011. Glacial-interglacial vegetation dynamics in South Eastern Africa coupled to sea surface temperature variations in the Western Indian Ocean. Climate of the past 7, 1209-1224.

Edmond, J.M., Boyle, E.D., Drummond, D., Grant, B., Mislick, T., 1978. Desorption of Barium in the plume of Zair (Congo) River. Netherlands Journal of Sea Research 12, 324-328.

EPICA-Community-members, 2006. One-to-one coupling of glacial climate variability in Greenland and Antarctica. Nature 444, 195-198.

Fallet, U., Brummer, G.-J., Zinke, J., Vogels, S., Ridderinkhof, H., 2010. Contrasting seasonal fluxes of planktonic foraminifera and impacts on

paleothermometry in the Mozambique Channel upstream of the Agulhas Current. Paleoceanography 25, PA4223.

Filippi, M.L., Talbot, M.R., 2005. The palaeolimnology of northern Lake Malawi over the last 25 ka based upon the elemental and stable isotopic composition of sedimentary organic matter. Quaternary Science Reviews 24, 1303-1328.

Garcin, Y., Vincens, A., Williamson, D., Guiot, J., Buchet, G., 2006. Wet phases in tropical southern Africa during the last glacial period. Geophysical Research Letters 33.

Hall, J.M., Chan, L.-H., 2004. Ba/Ca in *Neogloboquadrina pachyderma* as an indicator of deglacial meltwater discharge into the western Arctic Ocean. Paleoceanography 19, PA1017.

Holmgren, K., Lee-Thorp, J.A., Cooper, G.R.J., Lundblad, K., Partridge, T.C., Scott, L., Sithaldeen, R., Siep Talma, A., Tyson, P.D., 2003. Persistent millennial-scale climatic variability over the past 25,000 years in Southern Africa. Quaternary Science Reviews 22, 2311-2326.

Hönisch, B., Allen, K.A., Russell, A.D., Eggins, S.M., Bijma, J., Spero, H.J., Lea, D.W., Yu, J., 2011. Planktic foraminifers as recorders of seawater Ba/Ca. Marine Micropaleontology 79, 52-57.

Johnson, T.C., Brown, E.T., McManus, J., Barry, S., Barker, P., Gasse, F., 2002. A high-resolution paleoclimate record spanning the past 25,000 years in southern East Africa. Science 296, 113-132.

Johnson, T.C., Brown, E.T., Shi, J., 2011. Biogenic silica deposition in Lake Malawi, East Africa over the past 150,000 years. Palaeogeography, Palaeoclimatology, Palaeoecology 303, 103-109.

Kiefer, T., McCave, I.N., Elderfield, H., 2006. Antarctic control on tropical Indian Ocean sea surface temperature and hydrography. Geophysical Research Letters 33.

Kristen, I., Fuhrmann, A., Thorpe, J., Roehl, U., Wilkes, H., Oberhaensli, H., 2007. Hydrological changes in southern Africa over the last 20 ka as recorded in lake sediments from the Tswaing impact crater. South African Journal of Geology 110, 311-326.

Kristen, I., Wilkes, H., Vieth, A., Zink, K.G., Plessen, B., Thorpe, J., Partridge, T., Oberhänsli, H., 2010. Biomarker and stable carbon isotope analyses of sedimentary organic matter from Lake Tswaing: evidence for deglacial wetness and early Holocene drought from South Africa. Journal of Paleolimnology 44, 143-160.

Lea, D.W., Boyle, E.A., 1991. Barium in planktonic foraminifera. Geochimica et Cosmochimica Acta 55, 3321-3331.

Lea, D.W., Spero, H.J., 1994. Assessing the reliability of paleochemical tracers: barium uptake in the shells of planktonic foraminifera. Paleoceanography 9, 445-452.

Lee-Thorp, J.A., Holmgren, K., Lauritzen, S.E., Linge, H., Moberg, A., Partridge, T.C., Stevenson, C., Tyson, P.D., 2001. Rapid climate shifts in the southern African interior throughout the mid to late Holocene. Geophysical Research Letters 28, 4507-4510.

LeGrande, A.N., Schmidt, G.A., 2009. Sources of Holocene variability of oxygen isotopes in paleoclimate archives. Climate of the Past 5, 441-455.

LeGrande, A.N., Schmidt, G.A., Shindell, D.T., Field, C.V., Miller, R.L., Koch, D.M., Faluvegi, G., Hoffmann, G., 2006. Consistent simulations of multiple proxy

responses to an abrupt climate change event. Proceedings of the National Academy of Sciences of the United States of America 103, 837-842.

Levi, C., Labeyrie, L., Bassinot, F., Guichard, F.o., Cortijo, E., Waelbroeck, C., Caillon, N., Duprat, J., de Garidel-Thoron, T., Elderfield, H., 2007. Low-latitude hydrological cycle and rapid climate changes during the last deglaciation. Geochem. Geophys. Geosyst. 8, Q05N12, doi:10.1029/2006GC001514.

Levitus, S., Boyer, T.P., 1994. World Ocean Atlas 1994 Volume 4: Temperature. U.S. Department of Commerce, Washington, D.C.

Locarnini, R.A., Mishonov, A.V., Antonov, J.I., Boyer, T.P., Garcia, H.E., 2010. World Ocean Atlas 2005, Volume 1: Temperature. , In: U.S. Government Printing Office, W., D.C., 182 pp. World Ocean Atlas 2005 (Ed.), NOAA Atlas NESDIS 61 ed. U.S. Government Printing Office, Washington, D.C., p. 182 pp. .

Lourantou, A., Lavric, J.V., Köhler, P., Barnola, J.-M., Paillard, D., Michel, M., Raynaud, D., Chappellaz, J., 2010. Constraint of the CO2 rise by new atmospheric carbon isotopic measurements during the last deglaciation. Global Biogeochemical Cycles 24, **GB2015, doi:2010.1029/2009GB003545** .

Martin, P.A., Lea, D.W., 2002. A simple evaluation of cleaning procedures on fossil benthic foraminiferal Mg/Ca. Geochemistry, Geophysics, Geosystems 3, 1-8.

Meehl, G.A., Stocker, T.F., Collins, W.D., Friedlingstein, P., Gaye, A.T., Gregory, J.M., Kitoh, A., Knutti, R., Murphy, J.M., Noda, A., Raper, S.C.B., Watterson, I.G., Weaver, A.J., Zhao, Z.-C., 2007. Global Climate Projections, In: Solomon, S., D. Qin, M.M., Chen, Z., Marquis, M., Averyt, K.B., Tignor, M., Miller, H.L. (Eds.), Climate Change 2007: The Physical Science Basis. Contribution of Working Group I to the Fourth Assessment Report of the Intergovernmental Panel on

Climate Change. Cambridge University Press, Cambridge and New York, pp. 748-844.

Metwally, A. A., Scott, L., Neumann, F. H., Bamford, M. K. & Oberhänsli, H., 2014. Holocene palynology and palaeoenvironments in the Savanna Biome at Tswaing Crater, central South Africa. Palaeogeography, Palaeoclimatology, Palaeoecology 402, 125-135

Milliman, J.D., Meade, R.H., 1983. World-Wide Delivery of River Sediment to the Oceans. The Journal of Geology 91, 1-21.

Monnin, C., Jeandel, C., Cattaldo, T., Dehairs, F., 1999. The marine barite saturation state of the world´s oceans. Marine Geology 65, 253-261.

Monnin, E., Indermuhle, A., Dallenbach, A., Fluckiger, J., Stauffer, B., Stocker, T.F., Raynaud, D., Barnola, J.-M., 2001. Atmospheric CO2 Concentrations over the Last Glacial Termination. Science 291, 112-114.

Moore, S.M., 1997. High fluxes of radium and barium from the mouth of the Ganges-Brahmaputa River during low discharge suggest a large groundwater source. Earth and Planetary Science Letters 150, 141-150.

Pak, D.K., Lea, D.W., Kennett, J.P., 2004. Seasonal and interannual variation in Santa Barbara Basin water temperatures observed in sediment trap foraminiferal Mg/Ca. Geochemistry, Geophysics, Geosystems 5, Q12008.

Parrenin, F., Masson-Delmotte, V., Köhler, P., Raynaud, D., Paillard, D., Schwander, J., Barbante, C., Landais, A., Wegner, A., Jouzel, J., 2013. Synchronous Change of Atmospheric CO2 and Antarctic Temperature During the Last Deglacial Warming. Science 339, 1060-1063.

Partridge, T.C., de Menocal, P.B., Lorentz, S.A., Paiker, M.J., Vogel, J.C., 1997. Orbital forcing of climate over South Africa: A 200,000-year rainfall record from the Pretoria saltpan. Quaternary Science Reviews 16, 1125-1133.

Pausata, F.S.R., Battisti, D.S., Nisancioglu, K.H., Bitz, C.M., 2011. Chinese stalagmite [delta]18O controlled by changes in the Indian monsoon during a simulated Heinrich event. Nature Geosci 4, 474-480.

Powers, L., Werne, J.P., Vanderwoude, A.J., Sinninghe Damsté, J.S., Hopmans, E.C., Schouten, S., 2010. Applicability and calibration of the TEX86 paleothermometer in lakes. Organic Geochemistry 41, 404-413.

Reason, C.J.C., 2001. Subtropical Indian Ocean SST dipole events and southern African rainfall. Geophysical Research Letters 28, 2225-2227.

Reimer, P.J., Baillie, M.G.L., Bard, E., Bayliss, A., Beck, J.W., Blackwell, P.G., Ramsey, C.B., Buck, C.E., Burr, G.S., Edwards, R.L., Friedrich, M., Grootes, P.M., Guilderson, T.P., Hajdas, I., Heaton, T.J., Hogg, A.G., Hughen, K.A., Kaiser, K.F., Kromer, B., McCormac, F.G., Manning, S.W., Reimer, R.W., Richards, D.A., Southon, J.R., Talamo, S., Turney, C.S.M., van der Plicht, J., Weyhenmeye, C.E., 2009. Intcal09 and Marine09 radiocarbon age calibration curves, 0-50,000 years cal BP. Radiocarbon 51, 1111-1150.

Ridderinkhof, H., van der Werf, P.M., Ullgren, J.E., van Aken, H.M., van Leeuwen, P.J., de Ruijter, W.P.M., 2010. Seasonal and interannual variability in the Mozambique Channel from moored current observations. J. Geophys. Res. 115, C06010.

Rohling, E.J., Liu, Q.S., Roberts, A.P., Stanford, J.D., Rasmussen, S.O., Langen, P.L., Siddall, M., 2009. Controls on the East Asian monsoon during the last glacial cycle, based on comparison between Hulu Cave and polar ice-core records. Quaternary Science Reviews 28, 3291-3302.

Saji, N.H., Goswami, B.N., Vinayachandran, P.N., Yamagata, T., 1999. A dipole mode in the tropical Indian Ocean. Nature 401, 360-363.

Saraswat, R., Lea, D.W., Nigam, R., Mackensen, A., Naik, D.K., 2013. Deglaciation in the tropical Indian Ocean driven by interplay between the regional monsoon and global teleconnections. Earth and Planetary Science Letters 375, 166-175.

Schefuß, E., Kuhlmann, H., Mollenhauer, G., Prange, M., Patzold, J., 2011. Forcing of wet phases in southeast Africa over the past 17,000 years. Nature 480, 509-512.

Scholz, C.A., Johnson, T.C., Cohen, A.S., King, J.W., Peck, J.A., Overpeck, J.T., Talbot, M.R., Brown, E.T., Kalindekafe, L., Amoako, P.Y.O., Lyons, R.P., Shanahan, T.M., Castaneda, I.S., Heil, C.W., Forman, S.L., McHargue, L.R., Beuning, K.R., Gomez, J., Pierson, J., 2007. East African megadroughts between 135 and 75 thousand years ago and bearing on early-modern human origins. Proceedings of the National Academy of Sciences 104, 16416-16421.

Schott, F.A., Dengler, M., Schoenefeldt, R., 2002. The shallow overturning circulation of the Indian Ocean. Progress In Oceanography 53, 57-103.

Schulz, H., Lueckge, A., Emeis, K.-C., Mackensen, A., 2011. Variability of Holocene to Late Pleistocene Zambezi riverine sedimentation at the upper continental slope off Mozambique, 15 -21 degreeS. Marine Geology 286, 21-34.

Scott, L., Holmgren, K., Partridge, T.C., 2008. Reconciliation of vegetation and climatic interpretations of pollen profiles and other regional records from the last 60 thousand years in the Savanna Biome of Southern Africa. Palaeogeography, Palaeoclimatology, Palaeoecology 257, 198-206.

Scott, L., Neumann, F.H., Brook, G.A., Bousman, C.B., Norström, E., Metwally, A.A., 2012. Terrestrial fossil-pollen evidence of climate change during the last 26 thousand years in Southern Africa. Quaternary Science Reviews 32, 100-118.

Shakun, J.D., Clark, P.U., He, F., Marcott, S.A., Mix, A.C., Liu, Z., Otto-Bliesner, B., Schmittner, A., Bard, E., 2012. Global warming preceded by increasing carbon dioxide concentrations during the last deglaciation. Nature 484, 49-54.

Singh, S.P., Singh, S.K., Bhushan, R., 2013. Internal cycling of dissolved barium in water column of the Bay of Bengal. Marine Chemistry.

Southon, J., Kashgarian, M., Fontugne, M., Metivier, B., Yim, W.W.-S., 2002. Marine reservoir corrections for the Indian Ocean and Southeast Asia. Radiocarbon 44, 167-180.

Stager, J.C., Ryves, D.B., Chase, B.M., Pausata, F.S.R., 2011. Catastrophic Drought in the Afro-Asian Monsoon region during Heinrich Event 1. Science 331, 1299-1302.

Stuiver, M., Braziunas, T., 1993. Modeling atmospheric ^{14}C influences and ^{14}C ages of marine samples to 10,000 B.C. Radiocarbon 35, 137-189.

Thomas, D.S.G., Bailey, R., Shaw, P.A., Durcan, J.A., Singarayer, J.S., 2009. Late Quaternary highstands at Lake Chilwa, Malawi: Frequency, timing and possible forcing mechanisms in the last 44 ka. Quaternary Science Reviews 28, 526-539.

Toggweiler, J.R., Lea, D.W., 2011. Temperature differences between the hemispheres and ice age climate variability. Paleoceanography 25, PA2212.

Trauth, M.H., Deino, A.L., Bergner, A.G.N., Strecker, M.R., 2003. East African climate change and orbital forcing during the last 175 kyr BP. Earth and Planetary Science Letters 206, 297-313.

Truc, L. Chevalier, M., Favier, C., Cheddadi, R., Meadows, M. E., Scott, L., Carr, A. S., Smith, G. F., Chase, B. M., 2013. Quantification of climate change for the last 20,000years from Wonderkrater, South Africa: Implications for the long-term dynamics of the Intertropical Convergence Zone. *Palaeogeography, Palaeoclimatology, Palaeoecology* **386**, 575-587.

Ufkes, E., Fred Jansen, J. H. & Brummer, G.-J. A., 1998. Living planktonic foraminifera in the eastern South Atlantic during spring: Indicators of water masses, upwelling and the Congo (Zaire) River plume. Marine Micropaleontology 33, 27-53.

Ulrich, J., Pasenau, H., 1973. Untersuchungen zur Morphlogie des Schelfrandes vor Mozambique nördliche der Sambesi-Mündung. Deutsche Hydrographische Zeitschrift 26, 216-225.

van der Werf, P.M., van Leeuwen, P.J., Ridderinkhof, H., de Ruijter, W.P.M., 2010. Comparison between observations and models of the Mozambique Channel transport: Seasonal cycle and eddy frequencies. J. Geophys. Res. 115, C02002.

Waelbroeck, C., Labeyrie, L., Michel, E., McManus, J., Lambeck, K., Balbon, E., Labracherie, M., 2002. Sea-level and deep water temperature changes derived from benthic foraminifera isotopic records. Quaternary Science Research 21, 295-305.

Wang, Y.V., Larsen, T., Leduc, G., Andersen, N., Blanz, T., Schneider, R.R., 2013a. What does leaf wax δD from a mixed C3/C4 vegetation region tell us? Geochimica et Cosmochimica Acta 111, 128-139.

Wang, Y.V., Leduc, G., Regenberg, M., Andersen, N., Larsen, T., Blanz, T., Schneider, R.R., 2013b. Northern and southern hemisphere controls on seasonal

sea surface temperatures in the Indian Ocean during the last deglaciation. Paleoceanography, doi:10.1002/palo.20053.

Webster, P.J., Moore, A.M., Loschnigg, J.P., Leben, R.R., 1999. Coupled ocean-atmosphere dynamics in the Indian Ocean during 1997-98. Nature 401, 356-360.

Weijers, J.W.H., Schouten, S., Spaargaren, O.C., Sinninghe Damste, J.S., 2006. Occurrence and distribution of tetraether membrane lipids in soils: Implications for the use of the TEX86 proxy and the BIT index. Organic Geochemistry 37, 1680-1693.

Weldeab, S., 2012. Bipolar modulation of millennial-scale West African monsoon variability during the last glacial (75,000–25,000 years ago). Quaternary Science Reviews 40, 21-29.

Weldeab, S., Lea, D.W., Schneider, R.R., Andersen, N., 2007a. 155,000 years of West African monsoon and ocean thermal evolution. Science 316, 1303-1307.

Weldeab, S., Lea, D.W., Schneider, R.R., Andersen, N., 2007b. Centennial scale climate instabilities in a wet early Holocene West African monsoon. Geophysical Research Letters 34.

Williamson, D., Jelinowska, A., Kissel, C., Tucholka, P., Gibert, E., Gasse, F., Massault, M., Taieb, M., Van Campo, E., Wieckowski, K., 1998. Mineral-magnetic proxies of erosion/oxidation cycles in tropical maar-lake sediments (Lake Tritrivakely, Madagascar): paleoenvironmental implications. Earth and Planetary Science Letters 155, 205-219.

Xu, J., Holbourn, A., Kuhnt, W.G., Jian, Z.M., Kawamura, H., 2008. Changes in the thermocline structure of the Indonesian outflow during Terminations I and II. Earth and Planetary Science Letters 273, 152-162.

1

2

Figure captions

Figure 1: Sampling locations and annually averaged hydrographic characteristics in the southern tropical Indian Ocean. Upper panel shows the Zambezi basin, core locations (black diamonds) of GeoB9307-3 (18°33.90'S, 37°22.80'E, water depth 542 m) and GeoB9310-4 (19°12.11`S, 37°02.49'E, water depth 543 m), sites of seawater sampling (white diamonds), sites of foraminifer sampling from the water column (black dots in white diamonds), and annual sea surface salinity pattern in the Mozambique Channel and off the Zambezi River (Locarnini et al., 2010). Lower panel shows annually averaged SST (Locarnini et al., 2010) and surface currents (Schott et al., 2002) that are of relevance for heat and salinity exchange in the tropical and southern Indian Ocean. SEC: Southern Equatorial Current, AC: Agulhas Current, ARC: Agulhas Return Current, SAC: South Atlantic Current. Location of MD01-2378 (Xu et al., 2008) in the eastern Indian Ocean is also indicated.

Figure 2: A) Relationship between seawater Ba (Ba/Ca) and sea surface salinity in Mozambique Channel surface water (samples taken in February/March, 2008). Note that samples with low salinity and high Ba are from runoff-influenced sites (see Figure 1). B) Mg/Ca in *G. ruber* tests (300-400µm) from plankton tows plotted versus temperature (0-30 m) measured via CTD between February 29th and March 9th, 2008. Continuous and dashed lines indicate the global calibration curve and its uncertainty, respectively (Anand et al., 2003; Dekens et al., 2002).

Figure 3: A) Radiocarbon-based age model control points of GeoB9307-3 (red diamonds) and GeoB9310-4 (blue dots) plotted versus sampling sediment depth. The final age model is based on fourth order polynomial fits: age (cal. kyr)= $-3E-10x(depth)^4 + 5E-7x(depth)^3 - 0.0003x(depth)^2 + 0.1043x(depth) - 0.2102$ for GeoB9307-3 and age (cal. kyr)= $7E-7x(depth)^4 - 3E-8x(depth)^3 – 5E-5x(depth)^2 + 0.0437x(depth) + 0.2892$ for GeoB9310-4, where depth is sediment depth in cm. B) Changes in sedimentation rate in GeoB9307-3 and GeoB9310-4 plotted versus calendar age model. Inset shows location of GeoB9307-3 (red diamond) and GeoB9310-4 (blue dot) relative to the Zambezi river mouth and paleo- Chinde-Zambezi Channel (Beiersdorf et al., 1980; Schulz et al., 2011).

Figure 4: Proxy parameters analyzed in *G. ruber* white (250-300 µm). A) $\delta^{18}O$, B) Mg/Ca and Mg/Ca-SST estimates. C) Uncorrected and D) corrected Ba/Ca (see text). Black lines in A, B), and D) between 0 and 14 kyr BP indicate binned data of GeoB9310-4 and GeoB9307-3 (bin size 200 yr); for sections older than 14 ka cal BP, black lines indicate in A, B), and D) unbinned data of GeoB9307-3. Green dots along the x-axis indicate ^{14}C-date-based age model control points and their uncertainties (Table 1).

Figure 5: Comparison of SST estimates based on Mg/Ca (this study, red line) and TEX86 (Schefuß et al. (2011), green line) analyzed in GeoB9307-3. Black lines indicate 5-point running average of SST estimates. Sedimentation rate of GeoB9307-3 core sediment is also shown (blue line). The variability of terrestrial organic matter (TOM), as indicated by the BIT-index, is shown (Schefuß et al., 2011) (black line). At times of significantly elevated input of TOM, the TEX86-derived SST is higher by up to ~3 °C as compared to the Mg/Ca-based SST. Throughout the Holocene, when the input of TOM was very low, the TEX86-derived and Mg/Ca-based SST estimates are in generally better agreement, although still offset.

Figure 6: SST estimates based on Mg/Ca analysis in tests of the planktonic foraminifera *G. ruber* from (A) the eastern tropical Indian Ocean (Xu et al., 2008) and (B) Mozambique Channel (this study, binned) and plotted versus calendar age (kyr BP); the black line in A) indicates a 5-point running average. Grey shaded areas indicate phases of low SST in the Mozambique Channel. C) Shows $\delta^{18}O$ time series analyzed in Dronning Maud Land (Antarctica) (EDML) ice core (EPICA-Community-members, 2006). D) Atmospheric CO_2 analyzed in Dome Concordia ice core (Antarctica), (Monnin et al., 2001), 8-17.5 kyr synchronized to GICC05 age scale (Lourantou et al., 2010).

Figure 7: A) black line indicates eustatic sea level changes derived from benthic foraminiferal $\delta^{18}O$ (Waelbroeck et al., 2002) and black dots relative sea level changes based on corals from several sites compiled by Clark et al. (2009) and from Tahiti (Deschamps et al., 2012). B) Ba/Ca analyzed in tests of the planktonic foraminifera *G. ruber* (250-300µm) from cores GeoB9307-3 and GeoB931904 (composited and binned: bin size 200 yr). C) Fe/Ca ratios analyzed in bulk sediment using XRF-scanning (Schefuß et al. 2011). D) Branched and isoprenoid tetraether (BIT) index used as indicator of relative soil organic matter contributions (Schefuß et al., 2011).

Figure 8: Comparison of paleo-environmental and thermal changes in southeastern Africa and in the tropical Indian Ocean. A) Changes in zonal Indian Ocean SST gradient established using the difference between the eastern (Xu et al., 2008: 13˚4.95'S, 121˚47.27'E) and western Indian Ocean SST records (this study). To establish the zonal SST gradient, the Xu et al (2008) record was digitally resampled at a constant interval of 200 years. B) SST record from the Mozambique Channel. C) Reconstructed intervals of Lake Chilwa high stands (Thomas et al., 2009). D) Temperature and sea level corrected

$\delta^{18}O$ of seawater. E) Relative runoff estimate of Zambezi runoff based on Ba/Ca analysis in tests of the planktonic foraminifera G. ruber. F) Pollen record (5-point running average) from Lake Tritrivakely in Madagascar indicating changes in moisture availability over the riverine and wind catchment of the lake (Williamson et al., 1998). G) Principal component (PC) analysis of pollen assemblage from Wonderkrater in South Africa (Scott et al., 2012). Dotted line: January (15th) insolation at 15°S (Berger and Loutre, 1991). Green shaded areas indicate wet phases in the Zambezi basin, as suggested by the Ba/Ca record and weakened east-west Indian Ocean SST gradient.

Table 1: 32 ^{14}C-dating of monospecific and mixed foraminiferal tests in samples from GeoB9307-3 and GeoB9310-4. ^{14}C-ages were converted to calendar ages using CALIB (version 6.10) (Stuiver and Reimer, 1993), Marine09 data set (Reimer et al., 2009), and a constant reservoir age correction of ΔR= 203±32 yr (Southon et al., 2002).

Table 2: Geographic position of MOCNESS sampling sites, Mg/Ca data analyzed in *G. ruber*, test size of analyzed *G. ruber*, as well as SST, SSS, and average values of temperature and salinity of water depth between the sea surface and 30 m below the sea surface measure using CTD.

Figure 1
Click here to download high resolution image

Weldeab et al.-Figure 1

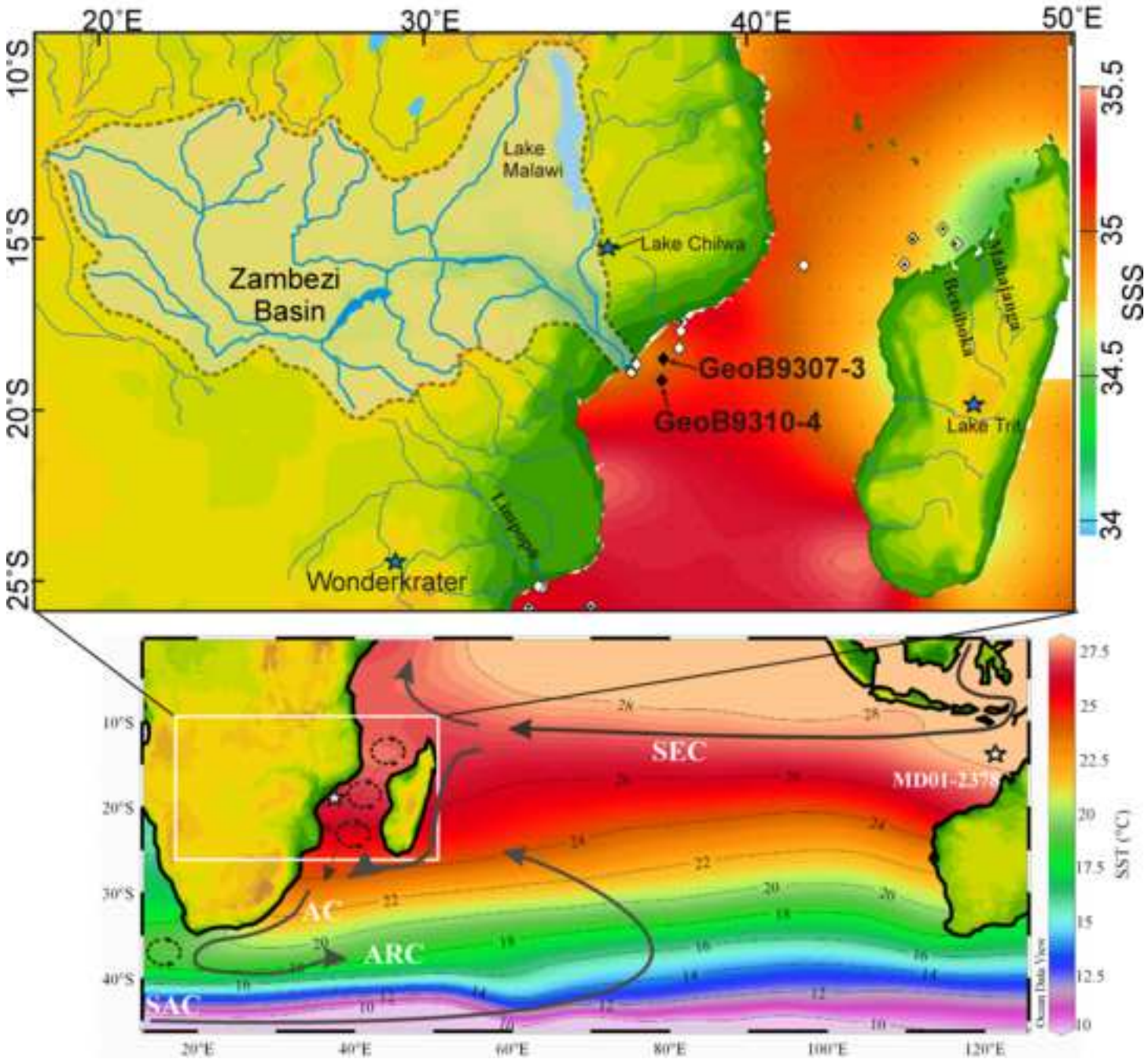

Figure 2
Click here to download high resolution image

Weldeab et al.-Figure 2

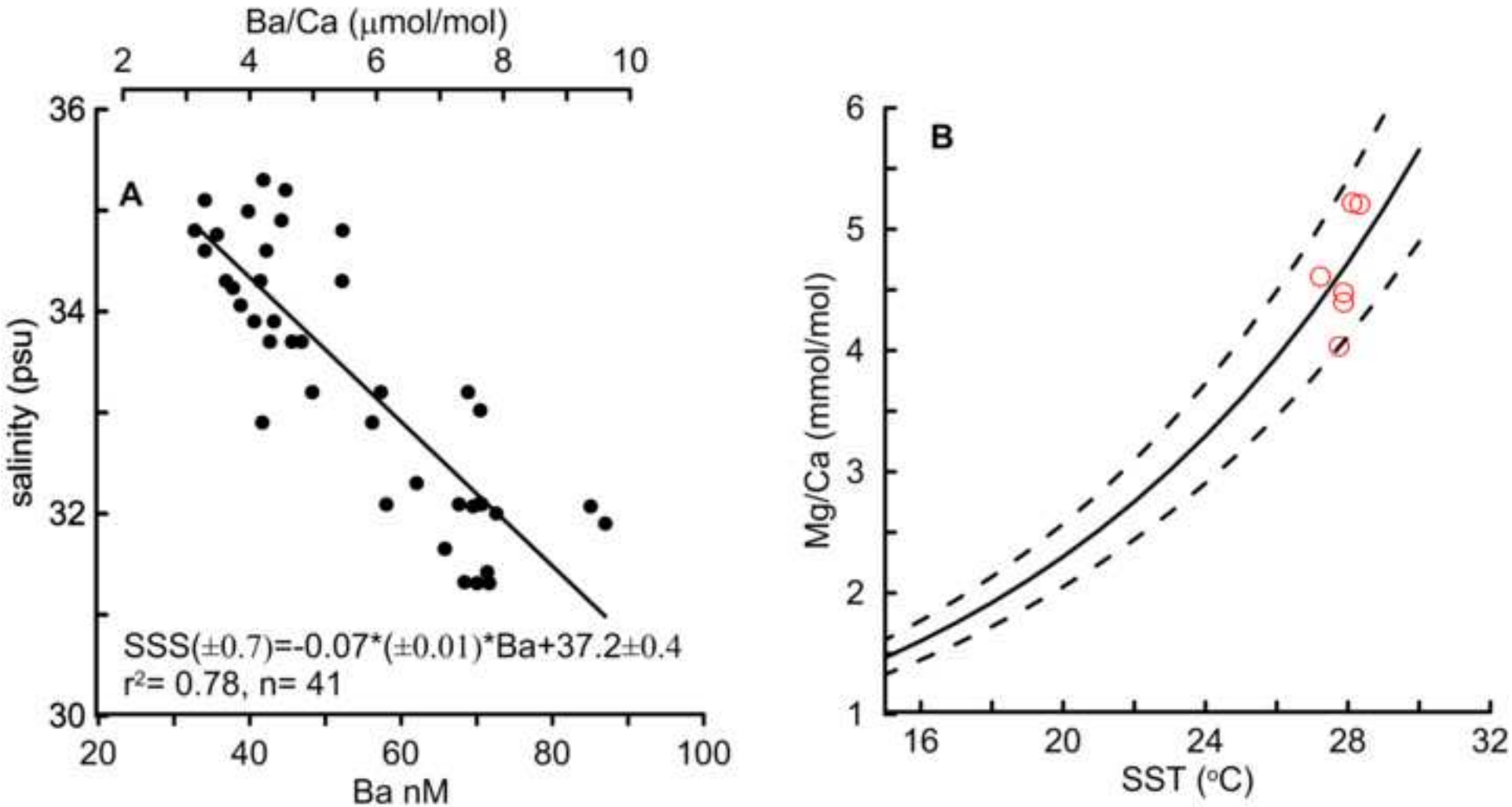

Figure 3
Click here to download high resolution image

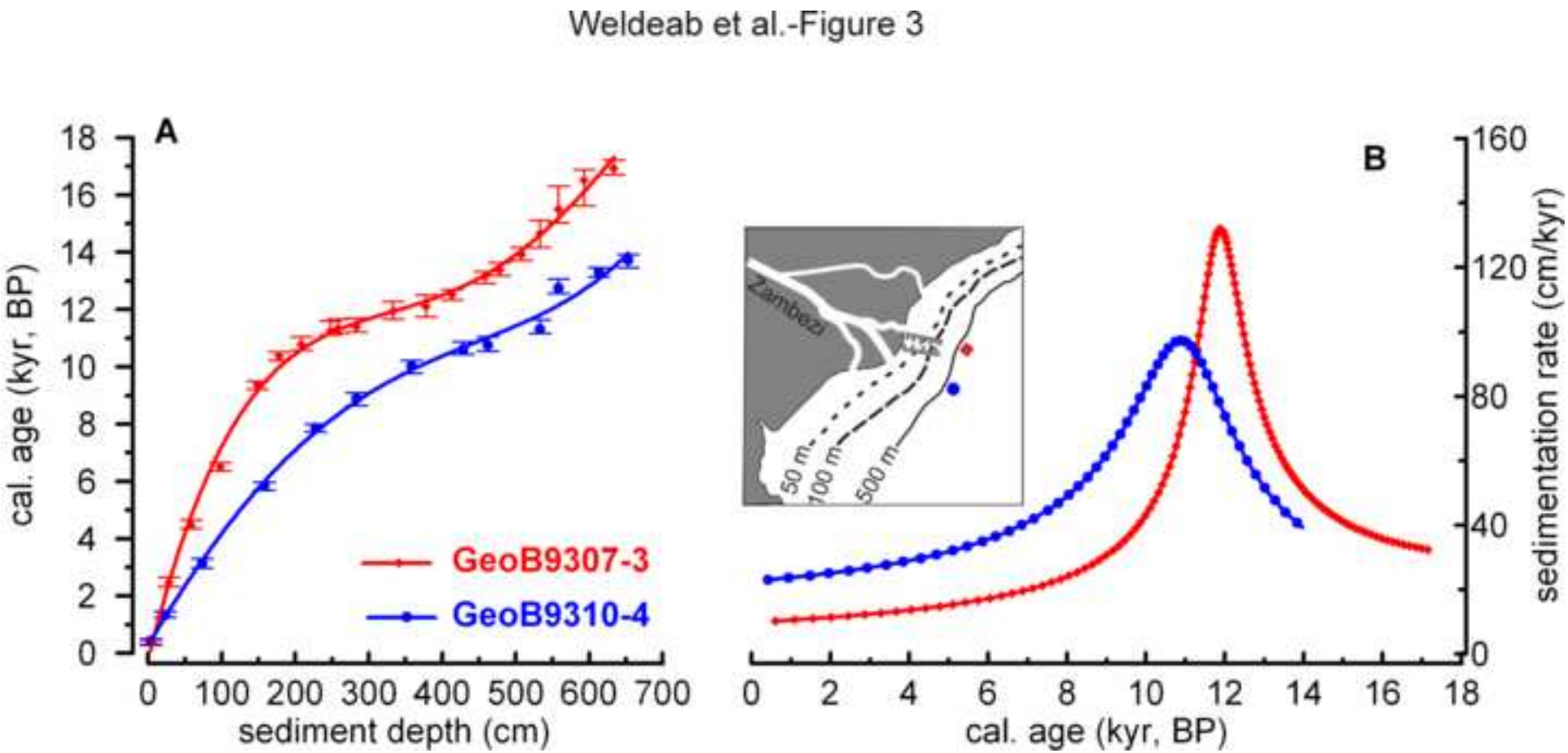

Figure 4
Click here to download high resolution image

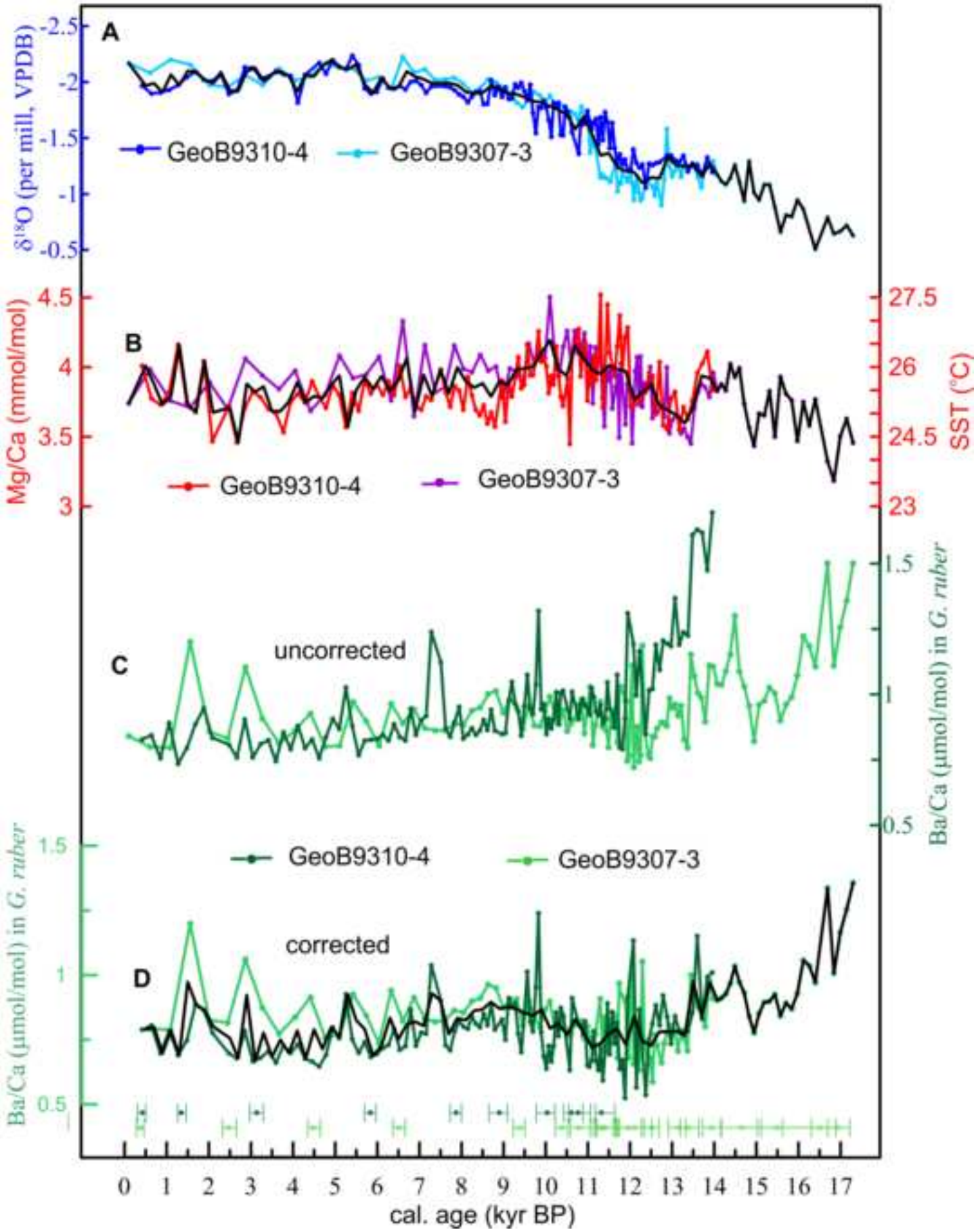

Figure 5
Click here to download high resolution image

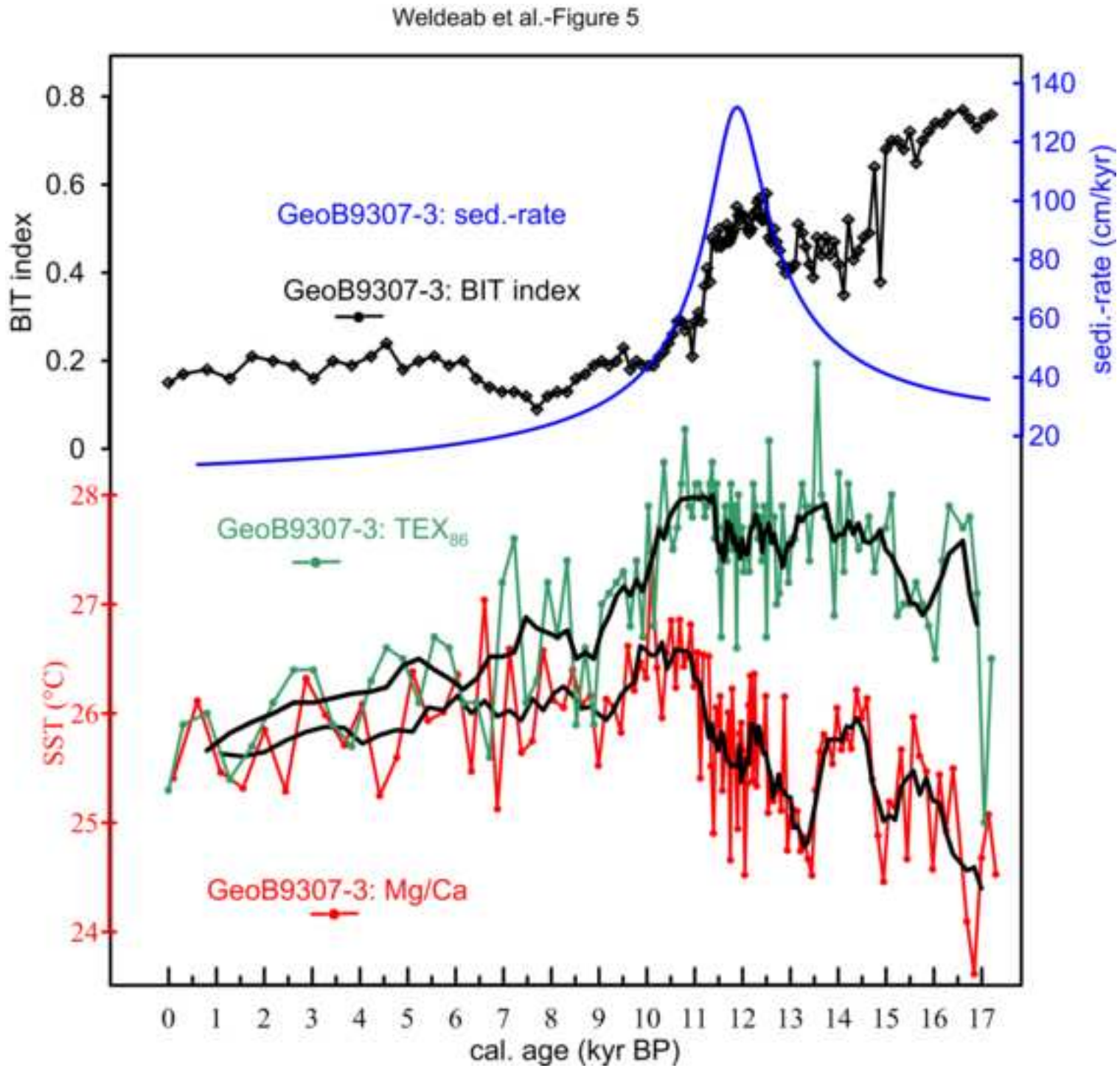

Figure 6
Click here to download high resolution image

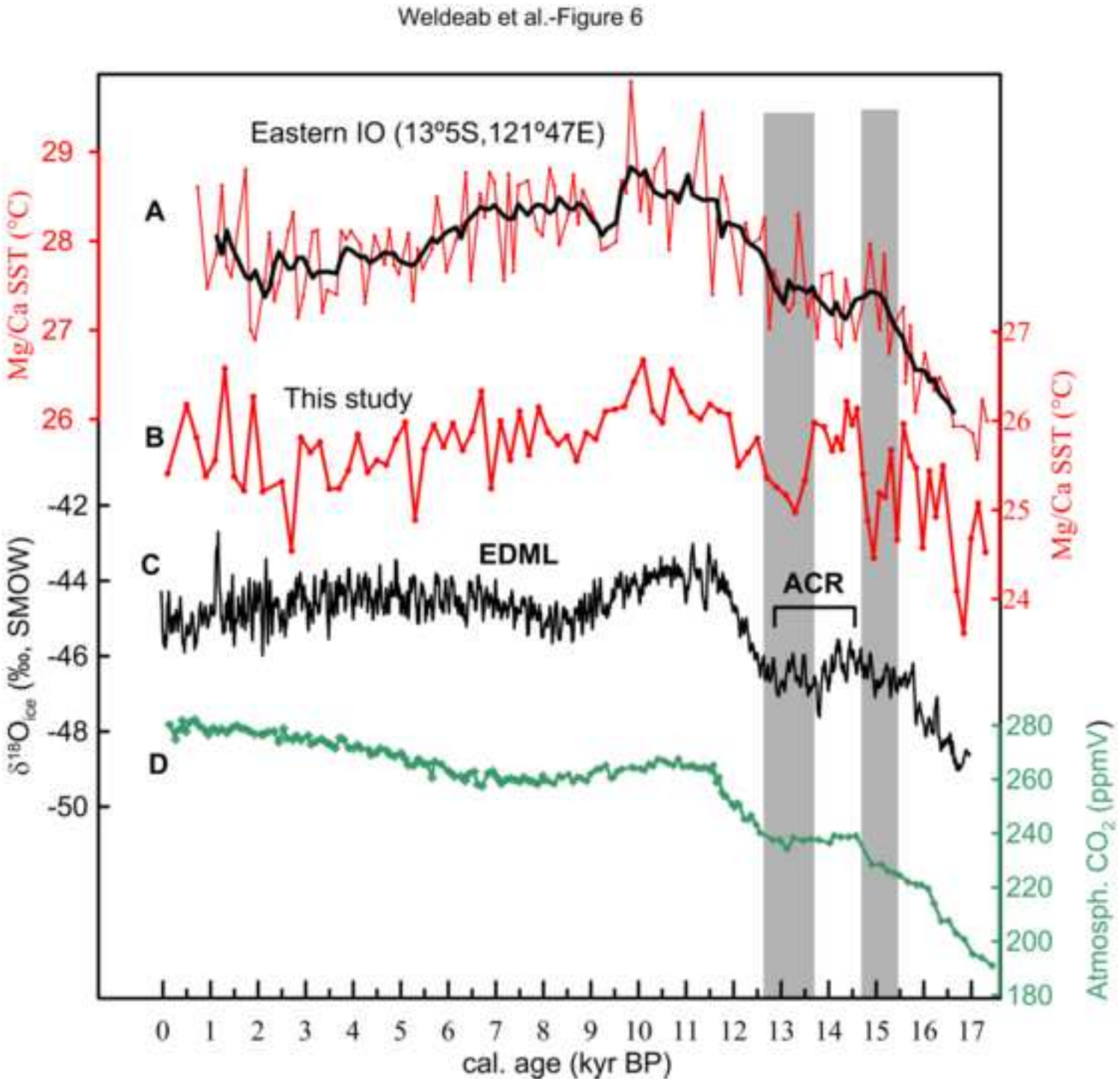

Figure 7
Click here to download high resolution image

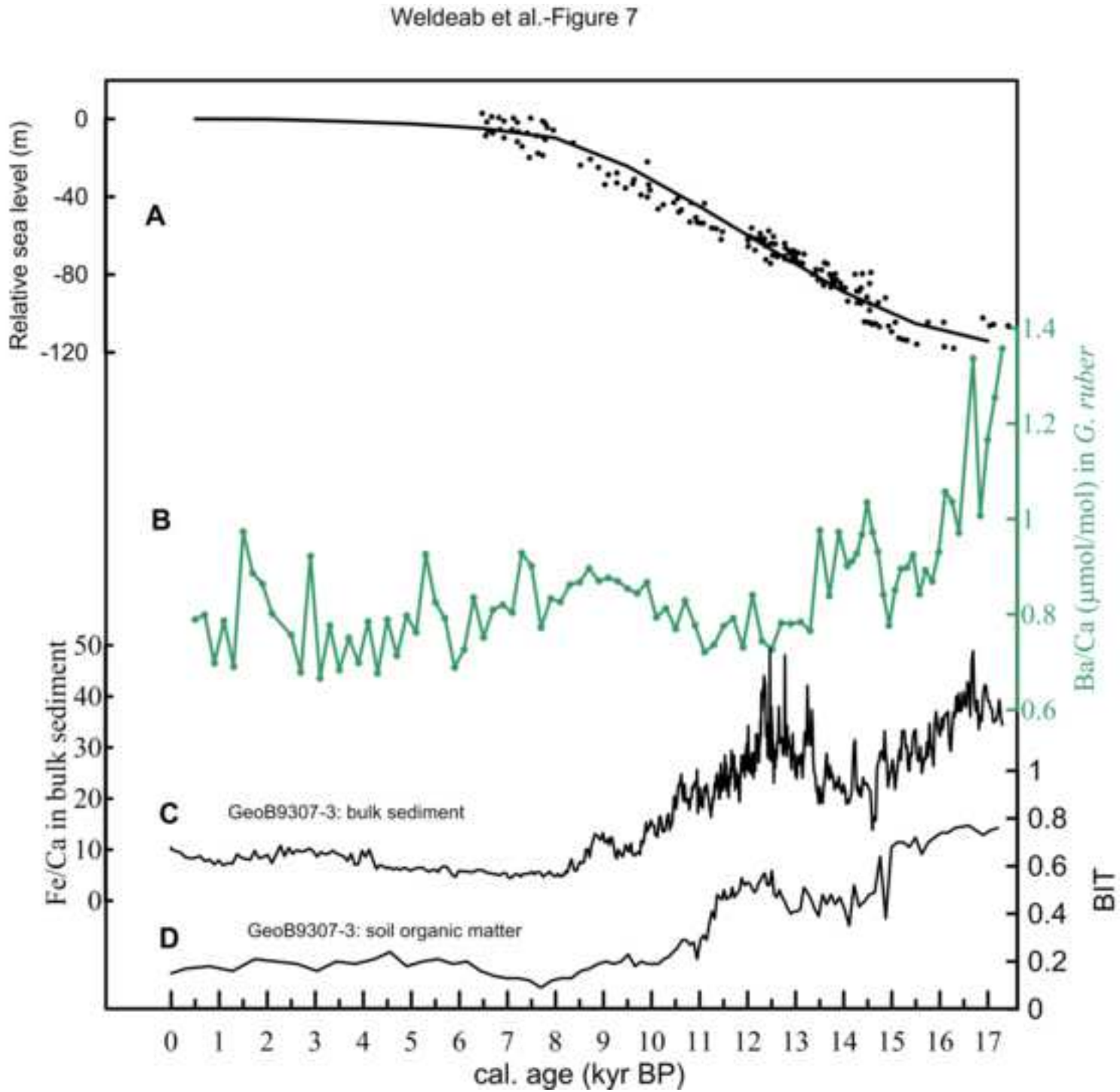

Figure 8
Click here to download high resolution image

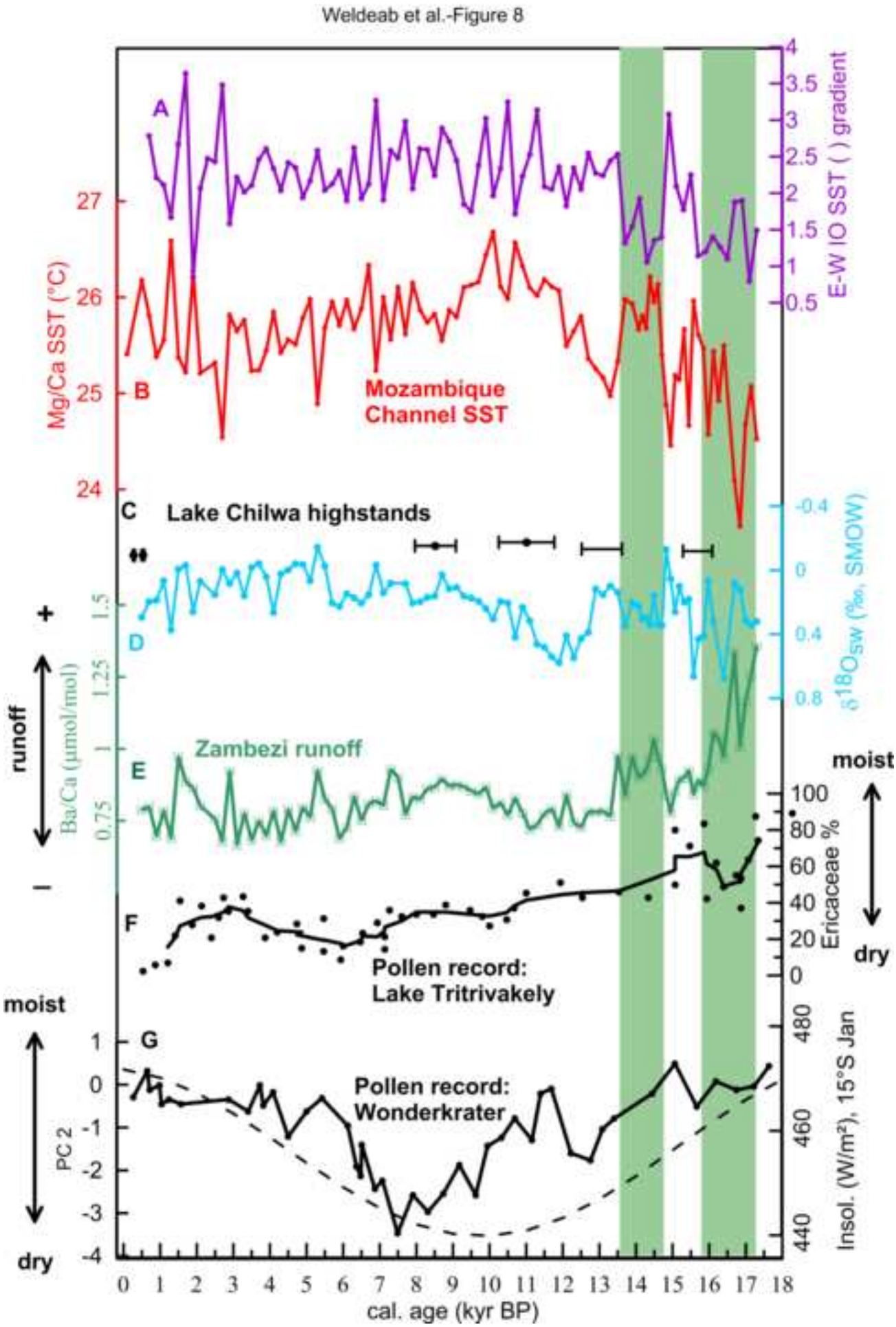

Weldeab et al.-Table 1
Click here to download Table: Weldeab et al.-Table 1.xlsx

Lab Code	Core	sediment depth (cm)	sample material	14C age, yr BP	uncertainty ± (yr, BP)
KIA 28442	GeoB9307-3	3	mixed plk. Forams	930	30
KIA 28441	GeoB9307-3	28	mixed plk. Forams	2945	45
KIA 28440	GeoB9307-3	58	mixed plk. Forams	4555	35
KIA 28438	GeoB9307-3	98	mixed plk. Forams	6290	50
KIA 28437	GeoB9307-3	148	mixed plk. Forams	8910	55
KIA 28436	GeoB9307-3	178	mixed plk. Forams	9730	60
KIA 28435	GeoB9307-3	208	mixed plk. Forams	10075	60
KIA 28434	GeoB9307-3	248	mixed plk. Forams	10470	60
KIA 28433	GeoB9307-3	258	mixed plk. Forams	10540	60
KIA 28431	GeoB9307-3	283	mixed plk. Forams	10570	60
KIA 28430	GeoB9307-3	333	mixed plk. Forams	10840	60
KIA 28429	GeoB9307-3	378	mixed plk. Forams	10920	70
KIA 28428	GeoB9307-3	413	mixed plk. Forams	11220	70
KIA 27758	GeoB9307-3	458	mixed plk. Forams	11870	80
KIA 27757	GeoB9307-3	478	mixed plk. Forams	12140	90
KIA 27755	GeoB9307-3	508	mixed plk. Forams	12680	90
KIA 27754	GeoB9307-3	533	mixed plk. Forams	13120	100
KIA 27753	GeoB9307-3	558	mixed plk. Forams	13530	100
KIA 27752	GeoB9307-3	593	mixed plk. Forams	14020	120
KIA 27751	GeoB9307-3	633	mixed plk. Forams	14450	110
KIA 27749	GeoB 9310-4	3	mixed plk. Forams	995	40
KIA 27748	GeoB 9310-4	23	G. Sacc	2005	30
KIA 27747	GeoB 9310-4	73	G. Sacc	3495	40
KIA 27746	GeoB 9310-4	158	G. Sacc	5665	45
KIA 27745	GeoB 9310-4	228	G. Sacc	7615	55
KIA 27744	GeoB 9310-4	283	G. Sacc	8540	60
KIA 27743	GeoB 9310-4	358	G. Sacc	9430	70
KIA 27742	GeoB 9310-4	428	G. Sacc	9940	70
KIA 27741	GeoB 9310-4	462	G. Sacc	10050	80
KIA 28424	GeoB 9310-4	533	G. sac+ruber+siph	10520	60
KIA 27740	GeoB 9310-4	558	G. Sacc	11460	120
KIA 28423	GeoB 9310-4	613	mixed plk	12060	70

Weldeab et al.-Table 2

Click here to download Table: Weldeab et al.-Table 2.xlsx

Station	Latitude	Longitude	sampling depth	Species	Test size	SST
			m		µm	°C
GIK16154-6	25°32.81`S	33°14.97`E	0-30	G ruber w	350	28.06
GIK16173-2	25°35.50´S	34°58.99`E	90-150	G ruber w	375-400	27.36
GIK16164-1	15°02.72`S	45°22.09`E	0-30	G ruber w	250-275	28.05
GIK16160-5	18°14.86`S	37°52.48`E	0-40	G ruber w	300	28.35
GIK16169-3	15°11.61`S	46°24.28`E	0-25	G ruber w	325-375	28.62
GIK16163-4	14°45.25`S	45°58.77`E	60-140	G ruber w	375-400	28.50

Highlights

- We present a 17 kyr record of SW Indian Ocean (IO) SST and climate of SE Africa
- The evolution of SW Indian deglacial SST followed the pace of Antarctic climate
- We propose that thermal link was established via shift of the austral westerlies
- Wet phases relate to elevated SW Indian Ocean SSTs and a weak zonal SST gradient
- Deglacial Antarctic climate likely had a strong control on SW IO SST and SE Africa climate

Supplemental Information

Weldeab et al.: Links between southwestern tropical Indian Ocean SST and precipitation over Southeastern Africa over the last 17 kyr

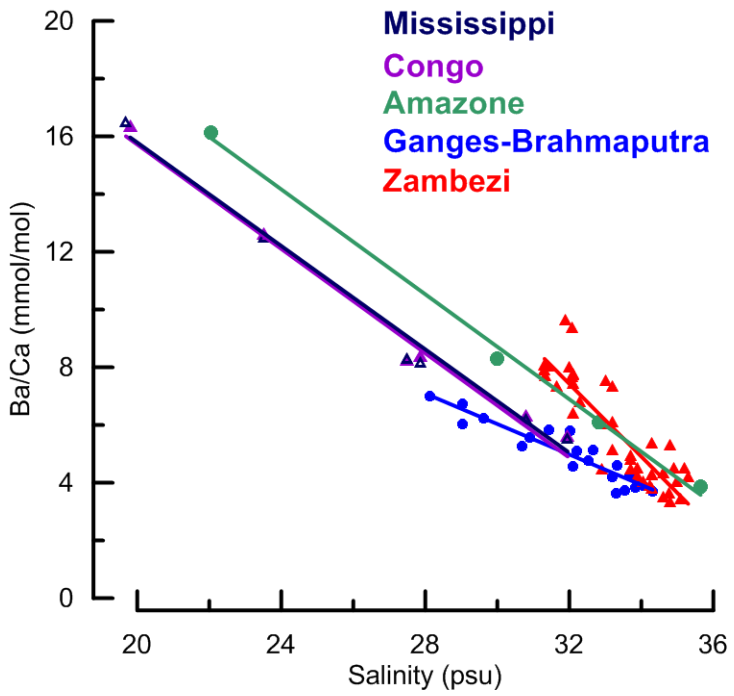

Figure S1: Relationship between dissolved Ba and sea surface salinity of water samples collected off the Mississippi River (dark blue), Amazon River (green), Congo River (Edmond et al., 1978) (purple), Ganges-Brahmaputra River (Singh et al., 2013) (blue), and Zambezi River (this study) (red). This plot demonstrates that the large-scale pattern of dissolved Ba distribution is controlled by the amount of runoff. The graph also shows that the geology of the catchment, weathering processes, and vegetation covers may

affect the relationship of dissolved Ba and runoff-induced salinity changes as indicated by the varying slopes of the linear fits.

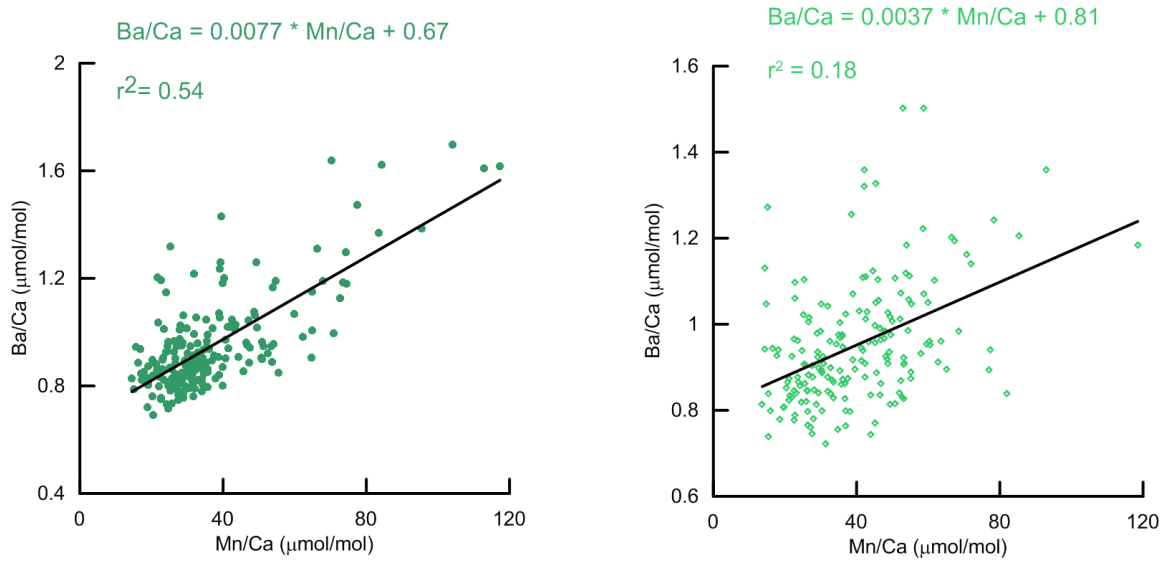

Figure S2: Ba/Ca and Mn/Ca correlation in *G. ruber* from GeoB9310-4 (left) and GeoB9307-3 (right).